

Part I

Preliminaries

Chapter 1

RBF Methods for PDEs

The process of solving partial differential equations (PDEs) using radial basis functions (RBFs) dates back to 1990 [34, 35]. However, at the core of all RBF methods lies the fundamental problem of approximation/interpolation. Some methods (e.g., global- and compact-RBF methods) apply RBFs to approximate derivatives directly. Others (e.g., RBF-generated Finite Differences) leverage the basis functions to generate weights for finite-differencing stencils, utilizing the weights in turn to approximate derivatives. Regardless, to track the history of RBF methods, one must look back to 1971 and R.L. Hardy’s seminal research on interpolation with multi-quadric basis functions [30].

As “meshless” methods, RBF methods excel at solving problems that require geometric flexibility with scattered node layouts in D -dimensional space. They naturally extend into higher dimensions without significant increase in programming complexity [19, 58]. In addition to competitive accuracy and convergence compared with other state-of-the-art methods [19, 20, 17, 58, 16], they also boast stability for large time steps.

This chapter is dedicated to summarizing the four-decade history of RBF methods leading up to the development of the RBF-generated Finite Differences (RBF-FD) method. Beginning with a brief introduction to RBFs and a historical survey, we attempt to classify related work into three types: global, compact, and local methods. Following this, the general approximation problem is introduced, with a look at the core of all three method classifications: RBF scattered-data interpolation.

Three collocation methods are presented: Kansa’s method, Fasshauer’s method and Direct collocation. Within the historical context of RBF methods we highlight extensions that lead to local interpolation matrices instead of a single global interpolation matrix. Finally, we discuss the most recent methods for solving PDEs, emphasizing RBF-FD as the focus of this work.

1.1 Survey of Related Work

In Radial Basis Function methods, radially symmetric functions provide a non-orthogonal basis used to interpolate between nodes of a point cloud. RBFs are univariate and a function of distance from a center point defined in \mathbb{R}^D , so they easily extend into higher dimensions without significant change in programming complexity. Examples of commonly used RBFs from the literature are provided in Table 1.1; 2D representations of the same functions can be found in Figure 1.1. Figure 1.2 illustrates the radial symmetry of RBFs—in this case, a Gaussian RBF—in the first three dimensions.

RBF methods are based on a superposition of translates of these radially symmetric functions, providing a linearly independent but non-orthogonal basis used to interpolate between nodes in D -dimensional space. The interpolation problem—referred to as *RBF scattered data interpolation*—seeks the unknown coefficients, $\mathbf{c} = \{c_j\}$, that satisfy:

Name	Abbrev.	Formula	Order (m)
Multiquadric	MQ	$\sqrt{1 + (\varepsilon r)^2}$	1
Inverse Multiquadric	IMQ	$\frac{1}{\sqrt{1 + (\varepsilon r)^2}}$	0
Gaussian	GA	$e^{-(\varepsilon r)^2}$	0
Thin Plate Splines	TPS	$r^2 \ln r $	2
Wendland (C^2)	W2	$(1 - \varepsilon r)^4(4\varepsilon r + 1)$	0

Table 1.1: Examples of frequently used RBFs based on [27, 13]. ε is the support parameter. All RBFs have global support. For compact support, enforce a cut-off radius (see Equation 1.1).

$$\sum_{j=1}^N \phi_j(r(\mathbf{x}))c_j = f(\mathbf{x}),$$

where $\phi_j(r(\mathbf{x}))$ is an RBF centered at $\{\mathbf{x}_j\}_{j=1}^N$. In theory the radial coordinate, $r(\mathbf{x})$, could be any distance metric, but is most often assumed to be $r(\mathbf{x}) = \|\mathbf{x} - \mathbf{x}_j\|_2$ (i.e., Euclidean distance), as it is here. The coefficients \mathbf{c} result in a smooth interpolant that collocates sample values $f(\mathbf{x}_j)$. An example of RBF interpolation in 2D using 15 Gaussians is shown in Figure 1.3.

RBFs have been shown in some cases to have exponential convergence for function approximation [13]. It is also possible to reformulate RBF methods as pseudospectral methods that have generated solutions to ill-posed problems for which Chebyshev-based and other pseudospectral methods fail [11]. However, as with all methods, RBFs come with certain limitations. For example, RBF interpolation is—in general—not a well-posed problem, so it requires careful choice of positive definite or conditionally positive definite basis functions (see [33, 13] for details).

RBFs depend on a shape or support parameter ϵ that controls the width of the function. The functional form of the shape function becomes $\phi(\epsilon r(\mathbf{x}))$. For simplicity in what follows, we use the notation $\phi_j(\mathbf{x})$ to imply $\phi(\epsilon \|\mathbf{x} - \mathbf{x}_j\|_2)$. Decreasing ϵ increases the support of the RBF and in most cases, the accuracy of the interpolation, but worsens the conditioning of the RBF interpolation problem [43]. This inverse relationship is widely known as the *Uncertainty Relation* [43, 33]. Fortunately, recent algorithms such as Contour-Padé [22] and RBF-QR [26, 24] allow for numerically stable computation of interpolants in the nearly flat RBF regime (i.e., $\epsilon \rightarrow 0$) where high accuracy has been observed [37, 27].

RBF methods for interpolation first appeared in 1971 with Hardy’s seminal research on multiquadrics [30]. In his 1982 survey of scattered data interpolation methods [28], Franke rated multiquadrics first-in-class against 28 other methods (3 of which were RBFs) [28]. Many other RBFs, including those presented in Table 1.1 have been applied in literature, but for PDEs in particular, none have rivaled the attention received by multiquadrics.

By 1990, the understanding of the scientific community regarding RBFs was sufficiently developed for collocating PDEs [34, 35]. PDE collocation seeks a solution of the form

$$(\mathcal{L}u)(x_i) = \sum_{j=1}^N \phi_j(x_i)c_j = f(x_i)$$

where \mathcal{L} is, in general, a nonlinear differential operator acting on $u(x)$. The solution $u(x)$ is expressed

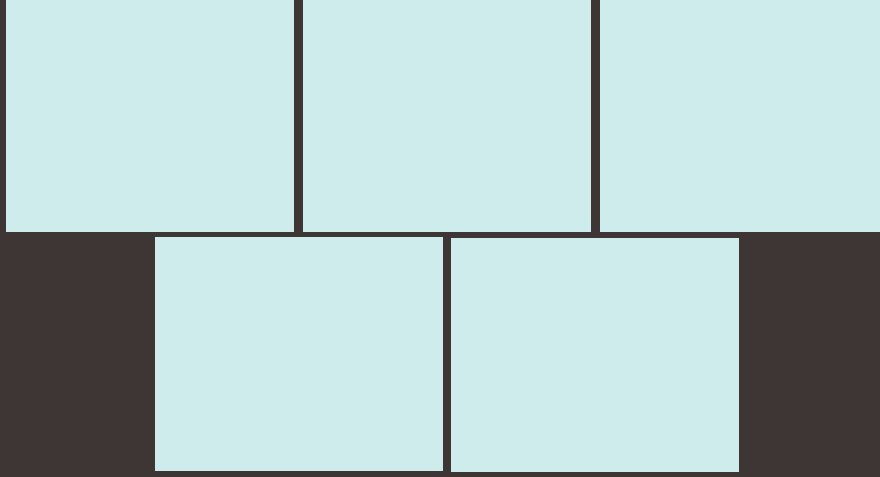


Figure 1.1: Example RBF shapes from Table 1.1 with parameter $\varepsilon = 1$.

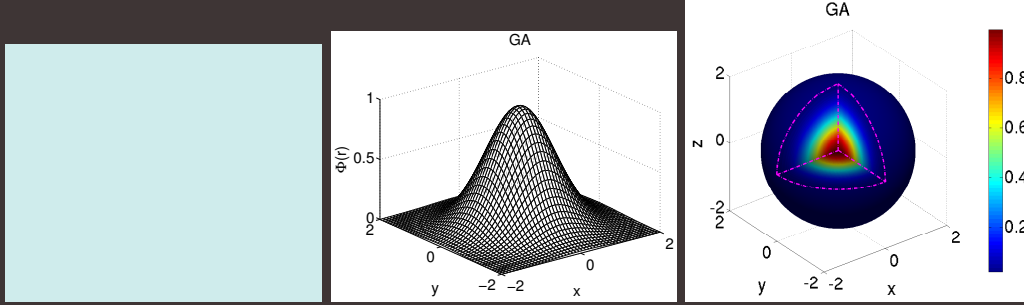


Figure 1.2: The Gaussian (GA) RBF (Table 1.1) with parameter $\varepsilon = 1$ and r in $D = 1, 2$ and 3 . as a linear combination of N basis functions $\phi_j(x)$, not necessarily RBFs:

$$u(x) = \sum_{i=1}^N \phi_j(x) c_j$$

As in the problem of RBF scattered data interpolation, $\mathbf{c} = \{c_j\}$ is the unknown coefficient vector. Under the assumption that \mathcal{L} is a linear operator, one can collocate the differential equation. Alternatively, individual derivative operators can be expressed as linear combinations of the unknowns u_j (leading to the RBF-FD methods). In all cases, a linear system of equations arises, with different degrees of sparsity, dependent on the chosen basis functions and how the various constraints are enforced. While we restrict the $\phi_j(x)$ to RBFs or various operators applied to the RBFs, we note that spectral methods, finite-element or spectral-element methods can be formulated in a similar way with different choices of basis functions. Of course, u can be a vector of unknown variables (\mathbf{c} then becomes a matrix).

In Table 1.3 we classify references according to their choice of collocation method and RBF interpolation type. There are three main categories of RBF interpolation; we list them in Table 1.2. The first is *Global* in the case that a single, large ($N \times N$) and dense matrix corresponding to globally supported RBFs is inverted; second, *Compact* if compactly supported RBFs are used to produce a single, large, but sparse matrix; and third, *Local* if compactly supported RBFs are used to produce many small but dense matrices with one corresponding to each collocation point. In all three cases the matrices are symmetric and with the correct choice of RBF they are at least conditionally positive definite.

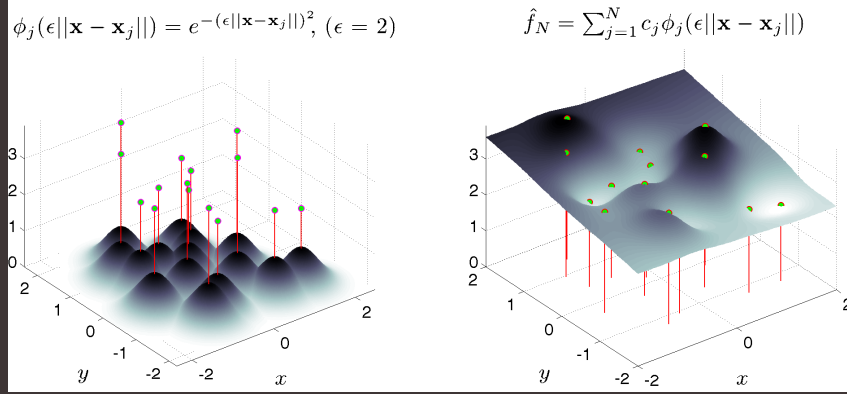


Figure 1.3: RBF interpolation using 15 translates of the Gaussian RBF with $\epsilon = 2$. One RBF is centered at each node in the domain. Linear combinations of these produce an interpolant over the domain passing through known function values.

Interpolation Type	Dense/Sparse A	Dim(A) ($N_S \ll N$)	# of A^{-1}	RBF Support
Global	Dense	$N \times N$	1	Global
Compact	Sparse	$N \times N$	1	Compact
Local	Dense	$N_S \times N_S$	N	Global/Compact

Table 1.2: RBF interpolation types and properties, assuming a problem with N nodes.

We note that three types of collocation occur throughout the RBF literature: Kansa’s unsymmetric collocation method [34, 35], Fasshauer’s symmetric collocation method [12], and the Direct collocation method [15]. While not a collocation method, RBF-FD represents the latest trend in solving PDEs with RBFs.

Prior to launching into derivation each RBF method, we first survey the classifications to highlight benefits, shortcomings, and to provide a brief historical context. A survey of related work in the RBF community that involves parallelization and optimization is deferred to Chapter 5.

1.1.1 Global RBF Methods

Kansa’s method [34, 35] (a.k.a. unsymmetric collocation) was the first RBF method for PDEs, and is still the most frequently used method. The idea behind Kansa’s method is that an approximate solution to the PDE can be found by finding an interpolant which satisfies the differential operator with zero residual at a set of *collocation points* (these coincide with the RBF centers). To find the interpolant, the differential equation is formulated as a two block (unsymmetric) linear system with: 1) the approximation of values at boundary points with boundary data only, and 2) the approximation of interior points by directly applying the differential operator. It was shown in [12, 31] that the unsymmetric linear system produced by Kansa’s method does not guarantee non-singularity; although it is also noted that in practice singularities are rare encounters [37].

The second alternative for RBF collocation, is based on Hermite scattered data interpolation (see [60]). The so-called *Fasshauer* or *Symmetric Collocation* method ([12]) performs a change of basis for the interpolant by directly applying the differential operator to the RBFs. It then collocates using the same approach as Kansa’s method [48, 37]. The resulting block structure of the linear system is symmetric and guaranteed to be non-singular [12]. In comparison to Kansa’s method, the

disadvantages of Fasshauer’s method include: a) requirement of higher order differentiability of the basis functions (to satisfy double application of the differential operator) and b) the linear system is larger and more complex to form [13]. As [31] points out, the possible existence of a singularity in Kansa’s method is not enough to justify the added difficulties of using Fasshauer’s method.

The last collocation method, *Direct Collocation*, was introduced by Fedoseyev, Friedman and Kansa [15] and satisfies the differential operator on the interior and the boundary. Larsson and Fornberg [37] observe that this third method has a matrix structure similar to that found in Kansa’s method; however, it is noted that the dimensions of the matrix blocks for each method differ. This is due to collocation constraints added for the differential operator applied to the boundary. Aside from the survey on RBF collocation presented by Larsson and Fornberg [37], no related work was found that applied, or investigated, this method further.

Both Kansa’s method and Fasshauer’s methods were shown in [11] to fit well in the generalized framework of pseudo-spectral methods with a subtle change in algorithm. While collocation methods explicitly compute the coefficients for a continuous derivative approximation, their alternates, referred to in literature as RBF-pseudospectral (RBF-PS) methods, never explicitly compute the interpolant coefficients. Instead, a differentiation matrix (DM) is assembled and used to approximate derivatives at the collocation points only [14]. Since most computational models are simply concerned with the solution at collocation points, the change to assemble DMs as in RBF-PS is organic.

Following the evolution of the RBF-PS algorithm, applications of global RBFs in the classic collocation sense (i.e., without the RBF-PS DMs) become impractical. This statement stems from the algorithmic complexity of each method. Global RBF methods result in full matrices [13]. The global collocation methods then scale on the order of $O(N^3)$ floating point operations (FLOPs) to solve for weighting coefficients on a given node layout, plus $O(N^2)$ to apply the weights for derivatives. If time-stepping is required, global collocation methods must recompute the time-dependent coefficients with additional cost dominated by $O(N^3)$ operations. RBF-PS methods have similar requirements for $O(N^3)$ operations to assemble the differentiation matrix and $O(N^2)$ to apply for derivatives. However, by avoiding time-dependent coefficients, RBF-PS methods only apply the differentiation matrix each time-step for $O(N^2)$ operations. As an aside, the $O(N^3)$ complexity for each method—typically due to an LU-decomposition, with subsequent forward- and back-solves—could be reduced. While not in mainstream use by the RBF community, [40] correctly points out that the use of iterative solvers could reduce complexity of preprocessing to the order of $O(N^2)$.

Hon et al. [32] employed Kansa’s method to solve shallow water equations for Typhoon simulation. In [20], Flyer and Wright employed RBF-PS (Kansa method) for the solution of shallow water equations on a sphere. Their results show that RBFs allow for longer time steps with spectral accuracy. The survey [16] by Flyer and Fornberg showcases RBF-PS (Kansa) out-performing some of the of the best available methods in geosciences, namely: Finite Volume, Spectral Elements, Double Fourier, and Spherical Harmonics. When applied to problems such as transport on the sphere [19], shallow water equations [20], and 3D mantle convection[58], RBF-PS consistently required fewer time steps, and a fraction of the nodes for similar accuracy [16].

1.1.2 Compactly Support RBFs

Thus far, all cases of collocation and interpolation mentioned have assumed globally supported RBFs. While global RBFs are well-studied and have nice properties, a major limitation is the large, dense system that must be solved. One alternative to global support is to use a set of compactly supported RBFs (CSRBFs) that are defined as:

$$\phi(r) = \begin{cases} \varphi(r) & r \in [0, 1] \\ 0 & r > 1 \end{cases} \quad (1.1)$$

where a radius is defined past which the RBF (in this case $\varphi(r)$) has no influence on the interpolant. Note that the radius can be scaled to fit a desired support. Methods that leverage CSRBFs produce

Method	RBF Interpolation Type		
	Global (Dense)	Compact (Sparse Global)	Local
Kansa's Method	[34, 35, 11, 22, 41, 31, 28, 20, 19, 32, 27, 37, 58, 16, 45]	[27, 55]	[10, 36, 54, 53]
Fasshauer's Method	[11, 12, 37]	[39]	[49, 50, 48]
Direct Collocation	[15, 37]		
RBF-FD	N/A	N/A	[59, 57, 46, 6, 56, 47, 7]

Table 1.3: Classification of references based on choice of RBF interpolation types and method for solving PDEs. References may appear in multiple cells according to the breadth of their research.

a global interpolation matrix that is *sparse* and therefore results in a system that is more efficiently assembled and solved [13]. The actual complexity estimate of the CSRBF method depends on the sparsity of the problem as well as the ordering of the assembled system. Assuming $n \ll N$ where n represents the number of nodes in support, [63] approximates the complexity as dominated by $O(N)$ for properly structured systems within MATLAB, and the investigation in [40] found $O(N^{1.5})$ consistent with the estimate provided by their choice of general sparse solver package. Fasshauer [13] provides a stationary multilevel collocation method based on CSRBF with $O(N)$ complexity, but the method is plagued by poor convergence. In the context of CSRBFs, analogues to Kansa's method and Fasshauer's method are known by the names *radial point interpolation method (RPIM)* [55] and *radial point interpolation collocation method (RPICM)* [39], respectively. A more thorough survey of CSRBF history can be found in [13, 33].

CSRBFs have attracted a lot of attention in applications. For example, in the field of dynamic surface and image deformation, compact support allows for local transformations which do not induce global deformation (see e.g., [61, 38, 9]).

We note that sparsity and spectral accuracy cannot be achieved simultaneously.

1.1.3 Local RBF Methods

Around 2005, Šarler and Vertnik [54, 53] demonstrated that if compactly supported RBFs are chosen, the traditional global collocation matrix from Kansa's method, can be avoided altogether in favor of small localized collocation matrices defined for each node. Local collocation still faces possible ill-conditioning and singularities like global collocation, but make it easier to distribute computation across parallel systems. Also, the smaller linear systems can be solved with less conditioning issues. In [54], the authors consider 2D diffusion problems. Divo and Kassab [10] employ the method for Poisson-like PDEs including fluid flow and heat transfer. Kosec and Šarler [36] apply the same technique to solve coupled heat transfer and fluid flow problems.

In similar fashion, Stevens et al. [50] introduced a local version of Fasshauer's method called *local Hermitian interpolation*. The authors have applied their method to 3D soil problems based on transient Richards' equations [49, 50, 48].

1.1.4 RBF-FD

RBF-generated Finite Differences (RBF-FD) were first introduced by Tolstykh in 2000 [52], but it was the simultaneous, yet independent, efforts in [46], [51], [57] and [6] that gave the method

its real start. The RBF-FD method (and the RBF-HFD, “Hermite” equivalent [59]) is similar in concept to classical finite-differences (FD), but differs in that the underlying differentiation weights are exact for RBFs rather than polynomials. The method contrasts with global RBF methods in the sense that it does not interpolate the differential operator of the PDE. Instead, the RBF-FD method applies the differential operator to translates of the RBF in a small stencil/neighborhood of nodes. Solving the interpolation system in RBF-FD results in the set of generalized FD weights that approximate the differential quantity at the stencil center.

RBF-FD share many advantages with global RBF methods, like the ability to function without an underlying mesh, easily extend to higher dimensions and afford large time steps; however spectral accuracy is lost. Other advantages of RBF-FD include lower computational complexity together with high-order accuracy (6th to 10th order accuracy is common). As in FD, increasing the stencil size, n , increases the accuracy of the approximation.

In some ways, RBF-FD and global RBF methods are plagued by the same difficulties. For example, as the number of nodes in the stencil increases, so too does the ill-conditioning of the linear systems to be solved. Similarly, the most accurate weights occur when $\epsilon \rightarrow 0$, but values in that regime beget additional ill-conditioning problems—a recurrence of the *Uncertainty Relation* [43]. One key difference in the multiple independent RBF-FD origins was that Wright [57] was able to bypass ill-conditioning of RBF-FD and investigate its behavior in the limit as $\epsilon \rightarrow 0$ by means of the Contour-Padé algorithm.

Given N total nodes in the domain, N linear systems, each of size $n \times n$, are solved to calculate the differentiation weights. Since $n \ll N$, the RBF-FD preprocessing complexity is dominated by $O(N)$; significantly lower than the global RBF method ($O(N^3)$). The cost per time step is also $O(N)$. Although the complexity of RBF-PS has closed the gap between the two methods, RBF-FD squeaks by

RBF-FD have been successfully employed for a variety of problems including Hamilton-Jacobi equations [6], convection-diffusion problems [7, 48], incompressible Navier-Stokes equations [46, 8], transport on the sphere [25], and the shallow water equations [18]. Shu et al. [47] compared the RBF-FD method to Least Squares FD (LSFD) in context of 2D incompressible viscous cavity flow, and found that under similar conditions, the RBF-FD method was more accurate than LSFD, but the solution required more iterations of an iterative solver. RBF-FD was applied to Poisson’s equation in [56]. Chandhini and Sanyasiraju [7] studied it in context of 1D and 2D, linear and non-linear, convection-diffusion equations, demonstrating solutions that are non-oscillatory for high Reynolds number, with improved accuracy over classical FD. An application to Hamilton-Jacobi problems [6], and 2D linear and non-linear PDEs including Navier-Stokes equations [46] have all been considered.

1.2 Comparison of RBF Methods

We now detail RBF methods for PDEs leading up to the derivation of RBF-FD.

Following [41], consider a PDE expressed in terms of a (linear) differential operator, \mathcal{L} :

$$\begin{aligned}\mathcal{L}u &= f && \text{on } \Omega \\ u &= g && \text{on } \Gamma\end{aligned}$$

where Ω is the interior of the physical domain, Γ is the boundary of Ω and f, g are known explicitly. In the case of a non-linear differential operator, a Newton’s iteration, or some other method, can be used to linearize the problem (see e.g., [59]); of course, this increases the complexity of a single time step. Then, the unknown solution, u , which produces the observations on the right hand side can be approximated by an interpolant function u_ϕ expressed as a linear combination of radial basis

functions, $\{\phi_j(x) = \phi(\|x - x_j\|)\}_{j=1}^N$, and polynomial functions $\{P_l(x)\}_{l=1}^M$:

$$u_\phi(x) = \sum_{j=1}^N \phi_j(x)c_j + \sum_{l=1}^M P_l(x)d_l, \quad P_l(x) \in \Pi_p^D \quad (1.2)$$

where $\phi_j(x) = \phi(\|x - x_j\|)$ ($\|\cdot\|$ is standard Euclidean distance). The second sum represents a linear combination of polynomials that enforces zero approximation error when $u(x)$ is a polynomial of degree less than or equal to p . The variable D is the problem dimension (i.e., $u_\phi(x) \in \mathbb{R}^D$). To eliminate degrees of freedom for well-posedness, p should be greater than or equal to the order of the chosen RBF (see Table 1.1) [33]. Note that Equation 1.2 is evaluated at $\{x_j\}_{j=1}^N$ data points through which the interpolant is required to pass with zero residual. We refer to the x_j 's as *collocation points* (a.k.a. trial points), taken as the RBF centers. The test points, x , usually coincide with collocation points, although this is not a requirement.

To clarify the role of the polynomial part in Equation 1.2, it is necessary to put aside the PDE for the moment and consider only the problem of *scattered data interpolation* with Radial Basis Functions.

1.2.1 RBF Scattered Data Interpolation

Borrowing notation from [13, 33], we seek an interpolant of the form

$$f(x) = \sum_{j=1}^N \phi_j(x)c_j$$

where $f(x)$ is expressed as a scalar product between the unknown coefficient weights c_j and the radial basis functions $\phi_j(x)$.

To obtain the unknown coefficients, c_j , form a linear system in terms of the N RBF centers:

$$\begin{aligned} f(x) &= \sum_{j=1}^N c_j \phi_j(x) \quad \text{for } x = \{x_j\}_{j=1}^N \\ \begin{pmatrix} f \end{pmatrix} &= \begin{bmatrix} \phi \end{bmatrix} \begin{pmatrix} c \end{pmatrix} \end{aligned}$$

The invertibility of this system depends on the choice of RBF, so one typically chooses a function that is positive definite to avoid issues. It has been shown (see [13, 33]) that some choices of RBFs (e.g. multiquadrics and thin-plate splines [31]) are not positive definite and therefore there is no guarantee that the approximation is well-posed. A sufficient condition for well-posedness is that the matrix be *conditionally positive definite*. In [13], Fasshauer demonstrates that conditional positive definiteness is guaranteed when Equation 1.2 exactly reproduces functions of degree less than or equal to m . For RBF scattered data interpolation in one dimension, this can be achieved by adding a polynomial of order m with $M = \binom{m+1}{1}$ terms (e.g., x^0, x^1, \dots, x^m). For \mathbb{R}^2 , the terms would be: $1, x, y, xy, x^2y, xy^2, \dots, x^m y^{m-1}, x^{m-1} y^m, x^m y^m$. In \mathbb{R}^D , $M = \binom{m+D}{D}$ [33], giving

$$\begin{aligned} \sum_{j=1}^N c_j \phi_j(x) + \sum_{l=1}^M d_l P_l(x) &= f(x), \quad P_l(x) \in \Pi_m^D \\ \begin{bmatrix} \phi & P \end{bmatrix} \begin{pmatrix} c \\ d \end{pmatrix} &= \begin{pmatrix} f \end{pmatrix} \end{aligned} \quad (1.3)$$

where the second summation (referred to as *interpolation conditions* [33]) ensures the minimum degree of the interpolant. Refer to Table 1.1 for a short list of recommended RBFs and minimally

required orders of m . This document prefers the Gaussian RBF. Notice, in Equation 1.3, that the interpolation conditions add M new degrees of freedom, so we must provide M additional constraints to square the system. In this case:

$$\sum_{j=1}^N c_j P_l(x_j) = 0, \quad l = 1, \dots, M$$

or

$$P^T c = 0. \quad (1.4)$$

It is now possible again to write the interpolation problem as a linear system using Equations 1.4 and 1.4:

$$\underbrace{\begin{bmatrix} \phi & P \\ P^T & 0 \end{bmatrix}}_{A_{\mathcal{L}}} \begin{pmatrix} c \\ d \end{pmatrix} = \begin{pmatrix} f \\ 0 \end{pmatrix} \quad (1.5)$$

Equation 1.5, typically a dense system except in the case of RBFs with compact support, can be solved efficiently via standard methods like LU-decomposition. With the coefficients, the interpolant can be sampled at any test points, $\{x_i\}_{i=1}^n$, by returning to Equation 1.3:

$$f(x_i) = \sum_{j=1}^N c_j \phi_j(x_i) + \sum_{l=1}^M d_l P_l(x_i) \quad (1.6)$$

$$= \underbrace{\begin{bmatrix} \phi & P \end{bmatrix}}_B \begin{pmatrix} c \\ d \end{pmatrix} \bigg|_{x=x_i} \quad (1.7)$$

1.2.2 Reconstructing Solutions for PDEs

In the next few subsections, we will consider collocation equations based on this general form:

$$\begin{aligned} \mathcal{L}u_{\phi}(x) &= f(x) & \text{on } \Omega \\ \mathcal{B}u_{\phi}(x) &= g(x) & \text{on } \Gamma \end{aligned}$$

where the methods presented below will apply the differential operators, \mathcal{L} and \mathcal{B} , to different choices of u_{ϕ} and different sets of collocation points. In many applications \mathcal{L} is chosen as a differential operator (e.g., $\frac{\partial}{\partial x}$, ∇ , ∇^2) and $\mathcal{B} = I$ (i.e. identity operator for Dirichlet boundary conditions) for PDEs. For RBF scattered data interpolation, $\mathcal{L} = I$. There are also applications where \mathcal{L} is a convolution operator (see e.g., [4, 5]) capable of smoothing/de-noising a surface reconstructed from point clouds.

For all the methods to be presented a linear system is generated:

$$\begin{aligned} A_{\mathcal{L}} \begin{pmatrix} c \\ d \end{pmatrix} &= \begin{pmatrix} f \\ 0 \end{pmatrix} \\ \begin{pmatrix} c \\ d \end{pmatrix} &= A_{\mathcal{L}}^{-1} \begin{pmatrix} f \\ 0 \end{pmatrix} \end{aligned} \quad (1.8)$$

where matrix $A_{\mathcal{L}}$ depends on the choice of collocation method. Once the linear system is solved, the value $u(x)$ is reconstructed at the test points following Equation 1.7:

$$\begin{aligned} u(x) &= \begin{bmatrix} \phi & P \end{bmatrix} \begin{pmatrix} c \\ d \end{pmatrix} \bigg|_{x=x_i} \\ &= B A_{\mathcal{L}}^{-1} \begin{pmatrix} f \\ 0 \end{pmatrix} \end{aligned} \quad (1.9)$$

Likewise, to obtain differential quantities we have:

$$\begin{aligned}\mathcal{L}u(x) &= \begin{bmatrix} \mathcal{L}\phi & \mathcal{L}P \end{bmatrix} \begin{pmatrix} c \\ d \end{pmatrix} \Big|_{x=x_i} \\ &= B_{\mathcal{L}} A_{\mathcal{L}}^{-1} \begin{pmatrix} f \\ 0 \end{pmatrix}.\end{aligned}$$

1.2.3 PDE Methods

Now, since $u_{\phi}(x)$ from Equation 1.2 cannot (in general) satisfy the PDE everywhere, we enforce the PDE at a set of collocation points, which are distributed over both the interior and the boundary. Again, these points do not necessarily coincide with the RBF centers, but it is convenient for this to be true in practice.

Kansa's Method

The first global RBF method for PDEs, *Kansa's method* [34, 35], collocates the solution through known values on the boundary, while constraining the interpolant to satisfy the PDE operator on the interior. This is equivalent to choosing u_{ϕ} according to Equation 1.2. The resulting system is given by [41]; assuming that \mathcal{L} is a linear operator,

$$\mathcal{L}u_{\phi}(x_i) = \sum_{j=1}^N c_j \mathcal{L}\phi_j(x_i) + \sum_{l=1}^M d_l \mathcal{L}P_l(x_i) = f(x_i) \quad i = 1, \dots, n_I \quad (1.10)$$

$$\mathcal{B}u_{\phi}(x_i) = \sum_{j=1}^N c_j \mathcal{B}\phi_j(x_i) + \sum_{l=1}^M d_l \mathcal{B}P_l(x_i) = g(x_i) \quad i = n_I + 1, \dots, n \quad (1.11)$$

$$\sum_{j=1}^N c_j P_l(x_j) = 0 \quad l = 1, \dots, M \quad (1.12)$$

where n_I are the number of interior collocation points, with the number of boundary collocation points equal to $n - n_I$. First, observe that the differential operators are applied directly to the RBFs inside summations, rather than first solving the scattered data interpolation problem and then applying the operator to the interpolant. Second, since the basis functions are known analytically, it is possible (although sometimes painful) to derive $\mathcal{L}\phi$ (refer to [13] for RBF derivative tables); the same is true for the polynomials P_l .

We can now reformulate Kansa's method as the linear system:

$$\underbrace{\begin{bmatrix} \phi_{\mathcal{L}} & P_{\mathcal{L}} \\ \phi_{\mathcal{B}} & P_{\mathcal{B}} \\ P^T & 0 \end{bmatrix}}_{A_{\mathcal{L}}} \begin{pmatrix} c \\ d \end{pmatrix} = \begin{pmatrix} f \\ g \\ 0 \end{pmatrix} \quad (1.13)$$

where $\phi_{\mathcal{L}} = \mathcal{L}\phi$, $P_{\mathcal{L}} = \mathcal{L}P$ are the interior components (Equation 1.10), $\phi_{\mathcal{B}}$ and $P_{\mathcal{B}}$ are the boundary components (Equation 1.11), and $P^T = [P_{\mathcal{L}}^T \ P_{\mathcal{B}}^T]$ are constraints for both interior and boundary polynomial parts (Equation 1.12). From Equation 1.13 it should be clear why Kansa's method is also known as the *Unsymmetric* collocation method.

Recall that the matrix in Equation 1.13 has no guarantee of non-singularity [12]; however, singularities are rare in practice [37].

Fasshauer's Method

Fasshauer's method [12] addresses the problem of singularity in Kansa's method by assuming the interpolation to be Hermite. That is, it requires higher differentiability of the basis functions (they must be at least C^k -continuous if \mathcal{L} is of order k). Leveraging this assumption, Fasshauer's method chooses:

$$u_\phi(x_i) = \sum_{j=1}^{N_I} c_j \mathcal{L}\phi_j(x_i) + \sum_{j=N_I+1}^N c_j \mathcal{B}\phi_j(x_i) + \sum_{l=1}^M d_l P_l(x_i) \quad (1.14)$$

as the interpolant passing through collocation points. Note N_I is used here to specify the number of RBF centers in the interior of Ω . Here the interpolant is similar to Equation 1.2, but a change of basis functions is used for the expansion: $\mathcal{L}\phi_j(x)$ on the interior and $\mathcal{B}\phi_j(x)$ on the boundary.

Collocating (i.e., substituting Equation 1.14 into Equations 1.10-1.12) we get:

$$\begin{aligned} \sum_{j=1}^{N_I} c_j \mathcal{L}^2 \phi_j(x_i) + \sum_{j=N_I+1}^N c_j \mathcal{L}\mathcal{B}\phi_j(x_i) + \sum_{l=1}^M d_l \mathcal{L}P_l(x_i) &= f(x_i) \quad i = 1, \dots, n_I \\ \sum_{j=1}^{N_I} c_j \mathcal{B}\mathcal{L}\phi_j(x_i) + \sum_{j=N_I+1}^N c_j \mathcal{B}^2 \phi_j(x_i) + \sum_{l=1}^M d_l \mathcal{B}P_l(x_i) &= g(x_i) \quad i = n_I + 1, \dots, n \\ \sum_{j=1}^{N_I} c_j \mathcal{L}P_l(x_j) + \sum_{j=N_I+1}^N c_j \mathcal{B}P_l(x_j) &= 0 \quad l = 1, \dots, M \end{aligned} \quad (1.15)$$

which is reformatted as the linear system:

$$\underbrace{\begin{bmatrix} \phi_{\mathcal{L}\mathcal{L}} & \phi_{\mathcal{L}\mathcal{B}} & P_{\mathcal{L}} \\ \phi_{\mathcal{B}\mathcal{L}} & \phi_{\mathcal{B}\mathcal{B}} & P_{\mathcal{B}} \\ P_{\mathcal{L}}^T & P_{\mathcal{B}}^T & 0 \end{bmatrix}}_{A_{\mathcal{L}}} \begin{pmatrix} c \\ d \end{pmatrix} = \begin{pmatrix} f \\ g \\ 0 \end{pmatrix} \quad (1.16)$$

Note that $\phi_{\mathcal{L}\mathcal{L}}$ represents the first summation in Equation 1.15. The linear system generated by Fasshauer's method reveals an interesting structure: namely, the subscripts \mathcal{L} and \mathcal{B} show blocks of influence in the matrix. For example, the interior RBF centers influence collocation on the interior collocation points ($\phi_{\mathcal{L}\mathcal{L}}$), boundary centers influence collocation on the interior ($\phi_{\mathcal{L}\mathcal{B}}$), interior centers influence collocation on the boundary ($\phi_{\mathcal{B}\mathcal{L}}$), and so forth. In the case where the collocation points and RBF centers do not coincide, the subscripts would also indicate which set of points the operators are applied to [48].

The symmetry of Fasshauer's (*symmetric collocation*) method is apparent in Equation 1.16. Likewise, it is clear that the symmetric method requires more storage and computation to solve compared to Kansa's method. However, based on the assumption that collocation points coincide with RBF centers, the symmetry reduces storage requirements by half.

Direct Collocation

In *Direct collocation* (see [37, 15], the interpolant is chosen as Equation 1.2 (the same as Kansa's method). However, the Direct method collocates both the interior and boundary operators at the

boundary points:

$$\begin{aligned}
\sum_{j=1}^N c_j \mathcal{L} \phi_j(x_i) + \sum_{l=1}^M d_l \mathcal{L} P_l(x_i) &= f(x_i) \quad i = 1, \dots, n \\
\sum_{j=1}^N c_j \mathcal{B} \phi_j(x_i) + \sum_{l=1}^M d_l \mathcal{B} P_l(x_i) &= g(x_i) \quad i = 1, \dots, n_B = n - n_I \\
\sum_{j=1}^N c_j P_l(x_j) &= 0 \quad l = 1, \dots, M
\end{aligned} \tag{1.17}$$

Reformulating as a linear system we get:

$$\begin{bmatrix} \phi_{\mathcal{L}} & P_{\mathcal{L}} \\ \phi_{\mathcal{B}} & P_{\mathcal{B}} \\ P^T & 0 \end{bmatrix} \begin{pmatrix} c \\ d \end{pmatrix} = \begin{pmatrix} f \\ g \\ 0 \end{pmatrix} \tag{1.18}$$

While the final system in Equation 1.18 is structured the same as Kansa's method (Equation 1.13), careful inspection of the index i in Equations 1.10 and 1.17 reveals that Direct collocation produces a larger system.

RBF-PS

The RBF-PS applies the same logic as Kansa's and Fasshauer's collocation methods to form matrix $A_{\mathcal{L}}$. However, RBF-PS makes a subtle change to assume the solution, $u(x)$, is only required at collocation points [11, 13]. Then, extending Equation 1.9 for the discrete differentiation matrix, $D_{\mathcal{L}}$, gives:

$$\begin{aligned}
u(x) &= (BA_{\mathcal{L}}^{-1}) \begin{pmatrix} f \\ 0 \end{pmatrix} \\
&= D_{\mathcal{L}}^T \begin{pmatrix} f \\ 0 \end{pmatrix}.
\end{aligned} \tag{1.19}$$

Here, $D_{\mathcal{L}}$ is independent of the function $f(x)$ and is assembled by solving the multiple RHS linear system:

$$D_{\mathcal{L}} = A_{\mathcal{L}}^{-T} B^T \tag{1.20}$$

For assembly, an LU-decomposition can be used ($O(N^3)$) in preprocessing [58, 13]. Forward- and back-solves for the decomposition are applied immediately ($O(N^2)$) to complete assembly.

Since matrix $D_{\mathcal{L}}$ is independent of $u(x)$ and $f(x)$, it is only updated if RBF centers move—a compelling benefit for time-dependent problems with stationary nodes—otherwise the solution is given by an $O(N^2)$ matrix multiply. In contrast, global RBF collocation methods construct the LU factors of $A_{\mathcal{L}}$ in preprocessing, but must apply forward- and back-solves at each time-step ($O(N^2)$) to obtain weighting coefficients before the pre-multiply of B (additional $O(N^2)$ step) provides the solution.

1.2.4 Local Methods

In the methods above, globally supported RBFs were required. However, the latest trend is to use RBFs defined with some cut-off radius to enforce compact support. In some cases, authors have used the compact support to produce a single (large) sparse system for interpolation (see e.g.,

[55, 39, 9, 61, 38]). Other approaches use compact support to produce local linear systems defined at each collocation point. Examples of this include [54, 53] for Kansa’s method, [49, 50, 48] for Fasshauer’s method. To our knowledge no one has considered local Direct collocation. Also, instead of specifying a cut-off radius, some authors specify the exact stencil size (i.e., number of neighboring points to include); see e.g., [10, 48].

After observing the general structure of the symmetric and unsymmetric collocation methods above, it is necessary only to present the symmetric (i.e. Fasshauer’s) local method and note that in the unsymmetric case certain blocks will be zero allowing the system to shrink.

The formula for the interpolant local to the (k) -th collocation point (i.e., RBF center) is given by:

$$u_{\phi}^{(k)}(x_i) = \sum_{j(k)=1}^{N_I} c_j^{(k)} \mathcal{L}\phi_j(x_i) + \sum_{j(k)=N_I+1}^{N_S} c_j^{(k)} \mathcal{B}\phi_j(x_i) + \sum_{l=1}^M d_l^{(k)} P_l(x_i) \quad (1.21)$$

where N_S represents the number of points that defines the local stencil; N is possibly a function of the cut-off radius in the RBF, N_I is the number of interior stencil points (those points of the stencil that lie in the interior of Ω). The index j is a function of the stencil center k allowing the system to include a local neighborhood of stencil points.

Collocating produces a linear system with similar structure to the global collocation problem, but the dimensions are much smaller:

$$\begin{bmatrix} \phi_{\mathcal{L}\mathcal{L}} & \phi_{\mathcal{L}\mathcal{B}} & P_{\mathcal{L}} \\ \phi_{\mathcal{B}\mathcal{L}} & \phi_{\mathcal{B}\mathcal{B}} & P_{\mathcal{B}} \\ P_{\mathcal{L}}^T & P_{\mathcal{B}}^T & 0 \end{bmatrix} \begin{pmatrix} c^{(k)} \\ d^{(k)} \end{pmatrix} = \begin{pmatrix} f \\ g \\ 0 \end{pmatrix} \quad (1.22)$$

Solving this system gives an interpolant locally defined around the stencil center. Note that approximating the PDE solution $u(x)$ requires finding the stencil center nearest x , then using the local interpolant for that stencil. Since interpolation is local (i.e., $c_j^{(k)}$ ’s are unique to each RBF center), reconstructing the derivatives with Equation 1.10 is limited to an inner product for each center rather than the matrix-vector grouping possible with global RBFs. Note that because the interpolants are local, there is no notion of global continuity/smoothness of the solution.

1.2.5 RBF-FD

While most of the literature surrounding RBFs for PDEs involves collocation, an alternative method does exist: RBF-FD. RBF-FD is a hybrid of RBF scattered data interpolation and Finite Difference stencils. The idea behind finite-difference stencils is to express various derivative operators as a linear combination of the unknown functional values in the neighborhood of the point where an approximation to the derivative operator is desired. Common approximations such as upwind differencing, center differencing, higher order approximations, and even spectral operators, are of this form. A common approach to building such discrete operators is to form a local interpolant in a neighborhood of the target point, and simply differentiate it analytically. This is the approach taken in RBF-FD, which allows for stencils with irregular placement and number of nodes, and assigns their weights based on an RBF [57]. A detailed derivation is provided in the next chapter. Such an approach leads to very simple implementations of time-advancement schemes, whether explicit or implicit. The solution at the new time step is simply some linear—if \mathcal{L} is linear, nonlinear otherwise—combination of the unknown functional values (if implicit scheme) or known functional value (if explicit scheme).

Key challenges lie in the choice of grid, the choice of stencil, whether or not to change the support as a function of the stencil, how to guaranty the stability of the differentiation operator after discretization, etc.

1.2.6 Time Stepping

Until now we have assumed that the differential operator \mathcal{L} had no time dependency. However, many important problems are a function of time:

$$\frac{\partial u(x; t)}{\partial t} = \mathcal{L}u(x; t) \quad (1.23)$$

$$\mathcal{B}(u(x; t)) = g(x) \quad (1.24)$$

with some initial condition $u(x; 0) = f(x)$. Both collocation methods and RBF-FD methods can be used to discretize the right hand side. In the case of collocation, the coefficients c are now functions of time. On the other hand, it is the unknown functional values that are considered to be the unknown, time-dependent variables when RBF-FD is used.

The general approach for collocation methods is to first use the initial and boundary conditions to get an initial set of coefficients $c(t), d(t)$, whereas before, (c, d) denotes the list of unknown coefficients of the RBF basis functions and the monomials. Prior to spatial discretization, Equation 1.24 is updated using any of the standard methods for time-stepping, such as Euler, Crank-Nicholson, or higher order Runge-Kutta methods to name a few. Here we demonstrate the approach with the Euler method (which is explicit) for simplicity. In practice, a higher order method would be chosen, perhaps an implicit method. The Euler method can be written as

$$u(x; t_{n+1}) = u(x; t_n) + \Delta t(\mathcal{L}u(x; t_n)) \quad (1.25)$$

Since $u(x; 0) = u(x; t_0)$ is known as a function of $(c, d) = A^{-1}u(x; t_n)$, it is straightforward to compute the coefficients, and from there, $\mathcal{L}(u(x; t_n))$.

Equation 1.25 is solved via a two step algorithm:

1. solve Equation ?? to approximate $\mathcal{L}u(x; t_n)$ for the current time-step
2. update $u(x; t_{n+1})$

Initially, $A_{\mathcal{L}}A^{-1}$ is computed once during the first time-step, and the first part of the algorithm is reduced to an inner product to get $\mathcal{L}u(x; t_n)$. Once $u(x; t_{n+1})$ is updated, one repeats the procedure with $u(x; t_{n+1})$ as a new initial condition. For collocation methods, one must recompute all the coefficients at each timestep (i.e. recompute A^{-1}), which is expensive. On the other hand, for a static grid, $A_{\mathcal{L}}A^{-1}$ can be precomputed and there is no longer any need to work in coefficient space. In this case, we have a type of RBF-FD method, which is solely expressed in terms of functional values. Of course, in a "pure" RBF-FD method, one has expressions for the various derivatives and operators as a linear combination of functional values (the derived stencil being an implicit function of the RBFs and their location).

There is a huge literature on time-stepping schemes for finite-difference, finite-volume, spectral methods, etc., and many of these methods can be adopted to the solve time-dependent problems on meshless grids. Although there are surely issues that are particular to RBFS, we do not discuss them here. Instead, we will include our experiences in the final thesis.

For initial value problems with moving nodes, the coefficients must be updated at each time-step whether working with collocation or RBF-FD. We do not consider moving node problems in this thesis.

Part II

The RBF-FD Method

1.2.7 Recent Advances in Conditioning

Recently, Fornberg and Wright [22] presented the *Contour-Padé algorithm*, which allows for numerically stable computation of highly accurate interpolants for (very small) cases typically associated with ill-conditioning induced by nearly flat RBFs (i.e., $\epsilon \rightarrow 0$). Larsson and Fornberg [37] applied the algorithm to all three methods of collocation (Kansa's, Fasshauer's and Direct Collocation) with considerable gain in accuracy over solutions from classical second-order FD and a pseudospectral method. Note that currently, the Contour-Padé algorithm was only studied for global RBF interpolation, not for compact or local methods.

The *RBF-QR* method, an alternative for numerically stable computation in the limit as $\epsilon \rightarrow 0$, was introduced by Fornberg and Piret [26] in context of a sphere, and later extended to planar 2D problems in [23]. The RBF-QR method is simple to implement (less than 100 lines of Matlab code), and it allows solution of large problems that are typically ill-conditioned. Fornberg, Larsson and Flyer [23] successfully applied RBF-QR on large problems with 6000 nodes for globally supported basis functions. [Author's Note: add mention of bengt's latest: \[24, ?\]](#)

With these two algorithms, global RBF methods have overcome most ill-conditioning issues for small to mid-sized problems. Unfortunately, both Contour-Padé and RBF-QR fail for large enough problems due to ill-conditioning. As the number of RBFs increases beyond a few thousand nodes it is impossible to avoid ill-conditioning of the extremely large interpolation matrix.

This reveals the benefit of local methods, which decrease the number of RBFs and ill-conditioning. However, in the limit as local stencil size increases to include all nodes in a domain, the local and global method are equivalent; thus it is known that local methods also suffer extreme ill-conditioning around 2000 nodes per stencil [47]. To our knowledge, no research has yet been published that applies the RBF-QR method to RBF-FD stencils.

1.2.8 Parallel RBF Implementations

Parallel implementations of RBF methods currently rely on parallel domain decomposition. Depending on the implementation, domain decomposition not only accelerates solution procedures, but can decrease the ill-conditioning that plague all global RBF methods [10]. The ill-conditioning is reduced if each domain is treated as a separate RBF domain, and the boundary update is treated separately. Domain decomposition methods for RBFs were introduced by Beatson et al. [2] in the year 2000 as a way to increase problem sizes into the millions of nodes.

Divo and Kassab [10] used a domain decomposition method with artificial subdomain boundaries for their implementation of a local collocation method [10]. Subdomains are processed independently. The derivative values at artificial boundary points are averaged to maintain global consistency of physical values. Their implementation was designed for a 36 node cluster, but benchmarks and scalability tests are not provided.

Kosec and Šarler [36] used OpenMP to parallelize coupled heat transfer and fluid flow problems on a single workstation. Their test cases used local collocation, explicit time-stepping and Neumann boundary conditions. A speedup factor of 1.85x over serial execution was achieved by executing on two CPU cores; no results from scaling tests were provided.

Stevens et al. [50] mention a parallel implementation under development, but no document is available yet.

Additional RBF implementations are discussed at the end of this chapter in the context of parallel co-processing with the GPU.

In this work, we will add to the above experiences, with the added twist of incorporating an implementation on the GPU (see later chapters).

Chapter 2

The RBF-FD Method

This is followed by a description of Radial Basis Function-generated Finite Differences and examples of operators approximated by the method within this work.

The choice to study RBF-FD within this dissertation is motivated by two factors. First, RBF-FD represents one of the latest developments within the RBF community. The method was formally introduced in 2003 but has yet to obtain the critical-mass following necessary for the method's use in large-scale scientific models. Our goal throughout the dissertation has been to scale RBF-FD to complex problems on high resolution meshes, and to lead the way for its adoption in high performance computational geophysics. Second, RBF-FD inherits many of the positive features from global and local collocation schemes, but sacrifices others for the sake of significantly reduced computational complexity and increased parallelism. We capitalize on the inherent parallelism to develop a collection of multi-GPU test cases that span the compute nodes of a Top 500 supercomputer. Our effort leads the way for application of RBF-FD in the modern field of high performance computing where GPU accelerators will be key to breaching the exa-scale barrier in computing [1].

Rather than solely focus on the optimizations of said algorithms on the GPU, we dedicate significant attention to the practical application of RBF-FD to interesting problems in geophysics. This means we have walked a fine line between research topics to both apply the method to

2.1 Related Works

The following are related works on RBF-FD. Each needs to be incorporated in this text:

-

Chapter 3

RBF Methods for PDE Solutions

3.1 The RBF-generated Finite Differences Method

For the RBF-FD method, derivatives of $u(x)$ are weighted combinations of a small neighborhood of N_s nodes (i.e., a stencil with $N_s \ll N$):

$$\mathcal{L}u(x_1) \approx \sum_{j=1}^{N_s} c_j u(x_j)$$

where $\mathcal{L}u$ denotes a linear differential quantity over u (e.g., $\mathcal{L}u = \frac{du}{dx}$). Here, c_j are unknown, and obtained by enforcing the reconstruction:

$$\mathcal{L}\phi_j(x_1) = \sum_{i=1}^{N_s} c_i \phi_j(x_i) \quad \text{for } j = 1, 2, \dots, N_s$$

with $\mathcal{L}\phi_j$ provided by analytically applying the differential operator to the kernel function. This is equivalent to:

$$\begin{pmatrix} \phi_1(x_1) & \phi_1(x_2) & \cdots & \phi_1(x_{N_s}) \\ \phi_2(x_1) & \phi_2(x_2) & \cdots & \phi_2(x_{N_s}) \\ \vdots & \ddots & \ddots & \vdots \\ \phi_{N_s}(x_1) & \phi_{N_s}(x_2) & \cdots & \phi_{N_s}(x_{N_s}) \end{pmatrix} \begin{bmatrix} c_1 \\ c_2 \\ \vdots \\ c_{N_s} \end{bmatrix} = \begin{bmatrix} \mathcal{L}\phi_1(x_1) \\ \mathcal{L}\phi_2(x_1) \\ \vdots \\ \mathcal{L}\phi_{N_s}(x_1) \end{bmatrix} \quad (3.1)$$

$$\phi_s \vec{c} = \vec{\phi}_{\mathcal{L}_s}. \quad (3.2)$$

Solving Equation 3.2 for stencils weights, \vec{c} , and substituting into Equation 3.4 reveals the similarity between RBF-FD and the general problem of RBF interpolation (see Equation ?? and discussion):

$$\begin{aligned} \mathcal{L}u(x_1) &\approx (\phi_s^{-1} \vec{\phi}_{\mathcal{L}_s})^T \vec{u} \\ &\approx \vec{\phi}_{\mathcal{L}_s}^T \phi_s^{-T} \vec{u} \end{aligned}$$

Again, based on the choice of RBF, positive definiteness of the system is ensured by adding the same constraints as Equation ??, but note differential quantities for $\vec{\mathbb{P}}$ on the right hand side:

$$\begin{pmatrix} \phi_s & P \\ P^T & 0 \end{pmatrix} \begin{bmatrix} c \\ d \end{bmatrix} = \begin{bmatrix} \vec{\phi}_{\mathcal{L}_s} \\ \vec{\mathbb{P}}_{\mathcal{L}} \end{bmatrix}. \quad (3.3)$$

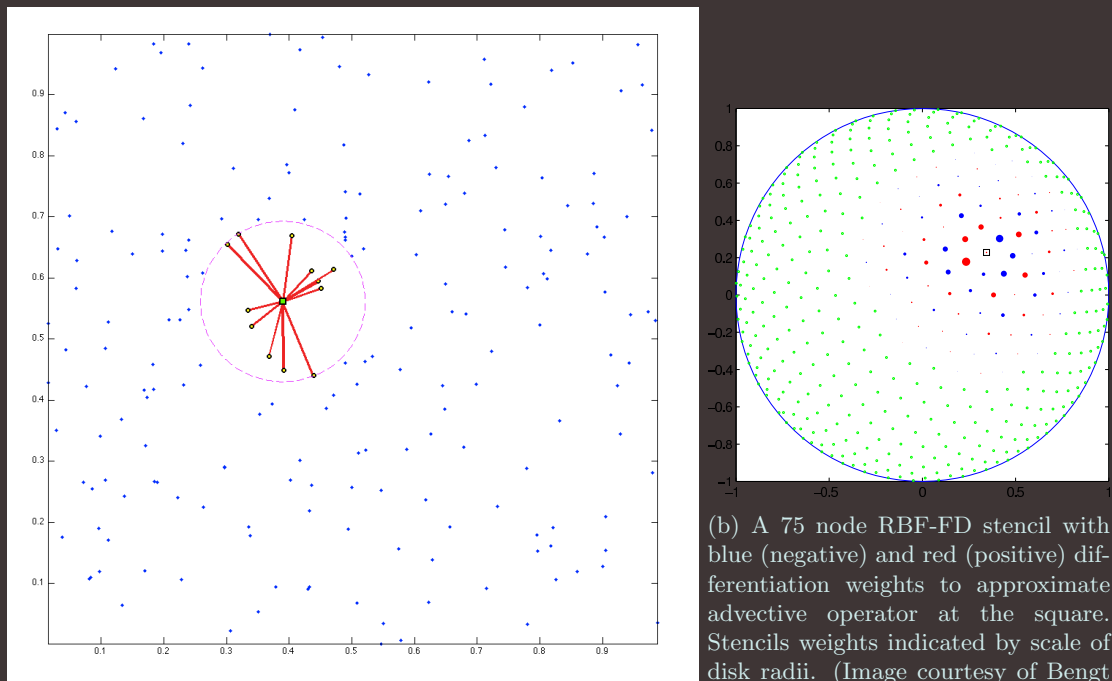
Equation 3.3 is strictly for the stencil centered at node x_1 . To obtain weights for all stencils in the domain, a total of N such systems must be solved.

3.2 Stencil-based Derivative Approximation

The RBF-FD method is similar to classical Finite Differences in that differential quantities at a single node referred to as a *center*, \mathbf{x}_j , is approximated by weighted combinations of function values at $n - 1$ neighboring nodes. The center node and its neighbors define a *stencil*, $\{\mathbf{x}\}_{i=1}^n$, in a localized (small) region or *neighborhood* of the domain.

Figure 3.1 provides two examples of RBF-FD stencils. First, Figure 3.1a illustrates a single stencil of size $n = 13$ in a domain of randomly distributed nodes. The stencil center is represented by a green square, with the 12 neighboring nodes connected via red edges. The purple circle, the minimum covering circle for the stencil, demonstrates that the stencil contains only the 12 nearest neighbors of the center node. In Figure 3.1b, a larger RBF-FD stencil of size $n = 75$ on the unit sphere is shown as red and blue disks surrounding the center represented as a square. Green disks are nodes outside of the stencil. The radii and color the red and blue disks represent the magnitude and sign of the RBF-FD weights determined to calculate a derivative quantity at the stencil center.

Weights for both classical Finite Difference and RBF-FD can be obtained through the solution of linear systems. In the case of Finite Difference, the system is a Vandermonde matrix. For RBF-FD the system is based on a symmetric distance matrix. [Author's Note: Need better description and ref](#) The key difference between FD and RBF-FD systems is the singularity that occurs when two nodes swap.



(a) A 13 node RBF-FD stencil of randomly distributed nodes. The stencil centered at the green square contains the 12 nearest neighbors contained within the minimum covering circle drawn in purple.

(b) A 75 node RBF-FD stencil with blue (negative) and red (positive) differentiation weights to approximate advective operator at the square. Stencils weights indicated by scale of disk radii. (Image courtesy of Bengt Fornberg and Natasha Flyer)

Figure 3.1: Examples of stencils computable with RBF-FD [Author's Note: Consider: show example FD stencil \(5pt with regular grid\)](#)

3.3 RBF-FD weights

Given a set of function values, $\{u(\mathbf{x}_j)\}_{j=1}^N$, on a set of N nodes $\{\mathbf{x}_j\}_{j=1}^N$, the operator \mathcal{L} acting on $u(\mathbf{x})$ evaluated at \mathbf{x}_j , is approximated by a weighted combination of function values, $\{u(\mathbf{x}_i)\}_{i=1}^n$, in a small neighborhood of \mathbf{x}_j , where $n \ll N$ defines the size of the stencil.

$$\mathcal{L}u(\mathbf{x})|_{\mathbf{x}=\mathbf{x}_j} \approx \sum_{i=1}^n c_i u(\mathbf{x}_i) + w_{n+1} p_0 \quad (3.4)$$

The RBF-FD weights, c_i , are found by enforcing that they are exact within the space spanned by the RBFs $\phi_i(\epsilon r) = \phi(\epsilon \|\mathbf{x} - \mathbf{x}_i\|)$, centered at the nodes $\{\mathbf{x}_i\}_{i=1}^n$, with $r = \|\mathbf{x} - \mathbf{x}_i\|$ being the distance between where the RBF is centered and where it is evaluated as measured in the standard Euclidean 2-norm. Various studies show [59, 21, 25, 18] that better accuracy is achieved when the interpolant can exactly reproduce a constant, p_0 . Assuming $p_0 = 1$, the constraint $\sum_{i=1}^n c_i = \mathcal{L}1|_{\mathbf{x}=\mathbf{x}_j} = 0$ completes the system:

$$\begin{pmatrix} \phi(\epsilon \|\mathbf{x}_1 - \mathbf{x}_1\|) & \phi(\epsilon \|\mathbf{x}_1 - \mathbf{x}_2\|) & \cdots & \phi(\epsilon \|\mathbf{x}_1 - \mathbf{x}_n\|) & 1 \\ \phi(\epsilon \|\mathbf{x}_2 - \mathbf{x}_1\|) & \phi(\epsilon \|\mathbf{x}_2 - \mathbf{x}_2\|) & \cdots & \phi(\epsilon \|\mathbf{x}_2 - \mathbf{x}_n\|) & 1 \\ \vdots & \vdots & \ddots & \vdots & \vdots \\ \phi(\epsilon \|\mathbf{x}_n - \mathbf{x}_1\|) & \phi(\epsilon \|\mathbf{x}_n - \mathbf{x}_2\|) & \cdots & \phi(\epsilon \|\mathbf{x}_n - \mathbf{x}_n\|) & 1 \\ 1 & 1 & \cdots & 1 & 0 \end{pmatrix} \begin{bmatrix} w_1 \\ w_2 \\ \vdots \\ w_n \\ w_{n+1} \end{bmatrix} = \begin{bmatrix} \mathcal{L}\phi(\epsilon \|\mathbf{x} - \mathbf{x}_1\|)|_{\mathbf{x}=\mathbf{x}_j} \\ \mathcal{L}\phi(\epsilon \|\mathbf{x} - \mathbf{x}_2\|)|_{\mathbf{x}=\mathbf{x}_j} \\ \vdots \\ \mathcal{L}\phi(\epsilon \|\mathbf{x} - \mathbf{x}_n\|)|_{\mathbf{x}=\mathbf{x}_j} \\ 0 \end{bmatrix}, \quad (3.5)$$

where w_{n+1} is ignored after the matrix in (3.5) is inverted. This $n \times n$ system solve is repeated for each stencil center \mathbf{x}_j , $j = 1 \dots N$, to form the N rows of the DM with n non-zeros ($n \ll N$) per row. As an example, if \mathcal{L} is the identity operator, then the above procedure leads to RBF-FD interpolation. If $\mathcal{L} = \frac{\partial}{\partial x}$, one obtains the DM that approximates the first derivative in x . In the context of time-dependent PDEs, the stencil weights remain constant for all time-steps when the nodes are stationary. Therefore, the calculation of the differentiation weights is performed once in a single preprocessing step of $O(n^3 N)$ FLOPs. Improved efficiency is achieved by processing multiple right hand sides in one pass, calculating the weights corresponding to all required derivative quantities (i.e., $\frac{\partial}{\partial x}$, $\frac{\partial}{\partial y}$, ∇^2 , etc.).

For each of the N small system solves of Equation (3.5), the n nearest neighbors to \mathbf{x}_j need to be located. This can be done efficiently using neighbor query algorithms or spatial partitioning data-structures such as Locality Sensitive Hashing (LSH) and k D-Tree. Different query algorithms often have a profound impact on the DM structure and memory access patterns. We choose a Raster (ijk) ordering LSH algorithm [?] leading to the matrix structure in Figures ?? and ??. While querying neighbors for each stencil is an embarrassingly parallel operation, the node sets used here are stationary and require stencil generation only once. Efficiency and parallelism for this task has little impact on the overall run-time of tests, which is dominated by the time-stepping. We preprocess node sets and generate stencils serially, then load stencils and nodes from disk at run-time. In contrast to the RBF-FD view of a static grid, Lagrangian/particle based PDE algorithms promote efficient parallel variants of LSH in order to accelerate querying neighbors at each time-step [42, 29].

Author's Note: Use of the 1's constraint is highly recommended. It keeps weights within magnitude 100, whereas not providing the constraint results in much higher magnitudes in the thousands or tens of thousands. Using first order monomials does not add benefit. Include examples of weights in 2D with 5 to 10 nodes.

3.4 Weight Operators

Throughout the development of our parallel code we have verified code correctness through the solution of a variety of PDEs. Here we provide a list of operators we have tested and their corresponding equations for the RHS of Equation 3.5 necessary to compute RBF-FD weights.

The standard first derivatives $\frac{\partial}{\partial x}, \frac{\partial}{\partial y}, \frac{\partial}{\partial z}$ are produced by the chain rule

$$\frac{\partial \phi}{\partial x} = \frac{dr}{dx} \frac{d\phi}{dr} = \frac{(x - x_j)}{r} \frac{d\phi}{dr} \quad (3.6)$$

$$\frac{\partial \phi}{\partial y} = \frac{dr}{dy} \frac{d\phi}{dr} = \frac{(y - y_j)}{r} \frac{d\phi}{dr} \quad (3.7)$$

$$\frac{\partial \phi}{\partial z} = \frac{dr}{dz} \frac{d\phi}{dr} = \frac{(z - z_j)}{r} \frac{d\phi}{dr} \quad (3.8)$$

where $\frac{\partial \phi}{\partial r}$ for the Gaussian RBFs is given by:

3.4.1 Laplacian (∇^2)

2D:

3D:

3.4.2 Laplace-Beltrami (Δ_S) on the Sphere

The ∇^2 operator can be represented in spherical polar coordinates for \mathbb{R}^3 as:

$$\nabla^2 = \underbrace{\frac{1}{r} \frac{\partial}{\partial r} \left(r^2 \frac{\partial}{\partial r} \right)}_{\text{radial}} + \underbrace{\frac{1}{r^2} \Delta_S}_{\text{angular}}, \quad (3.9)$$

where Δ_S is the Laplace-Beltrami operator—i.e., the Laplacian operator constrained to the surface of the sphere. This form nicely illustrates the separation of components into radial and angular terms.

In the case of PDEs solved on the unit sphere, there is no radial term, so we have:

$$\nabla^2 \equiv \Delta_S. \quad (3.10)$$

Although this originated in the spherical coordinate system, [58] introduced the following Laplace-Beltrami operator for the surface of the sphere:

$$\Delta_S = \frac{1}{4} \left[(4 - r^2) \frac{\partial^2}{\partial r^2} + \frac{4 - 3r^2}{r} \frac{\partial}{\partial r} \right], \quad (3.11)$$

where r is the Euclidean distance between nodes of an RBF-FD stencil and is independent of our choice of coordinate system.

3.4.3 Constrained Gradient ($P_x \cdot \nabla$) on the Sphere

Additionally following [20, 18], the gradient operator must also be constrained to the sphere with this projection matrix:

$$P = I - \mathbf{x}\mathbf{x}^T = \begin{pmatrix} (1 - x_1^2) & -x_1x_2 & -x_1x_3 \\ -x_1x_2 & (1 - x_2^2) & -x_2x_3 \\ -x_1x_3 & -x_2x_3 & (1 - x_3^2) \end{pmatrix} = \begin{pmatrix} P_{x_1} \\ P_{x_2} \\ P_{x_3} \end{pmatrix} \quad (3.12)$$

where \mathbf{x} is the unit normal at the stencil center.

The direct method of computing RBF-FD weights for the projected gradient for $\mathbf{P} \cdot \nabla$ is presented in [20]. When solving for the weights, we apply the projection on the right hand side of our small linear system. We let $\mathbf{x} = (x_1, x_2, x_3)$ be the stencil center, and $\mathbf{x}_k = (x_{1,k}, x_{2,k}, x_{3,k})$ indicate an RBF-FD stencil node.

Using the chain rule, and assumption that

$$r(\mathbf{x}_k - \mathbf{x}) = \|\mathbf{x}_k - \mathbf{x}\| = \sqrt{(x_{1,k} - x_1)^2 + (x_{2,k} - x_2)^2 + (x_{3,k} - x_3)^2},$$

we obtain the unprojected gradient of ϕ as

$$\nabla \phi(r(\mathbf{x}_k - \mathbf{x})) = \frac{\partial r}{\partial \mathbf{x}} \frac{\partial \phi(r(\mathbf{x}_k - \mathbf{x}))}{\partial r} = -(\mathbf{x}_k - \mathbf{x}) \frac{1}{r(\mathbf{x}_k - \mathbf{x})} \frac{\partial \phi(r(\mathbf{x}_k - \mathbf{x}))}{\partial r}$$

Applying the projection matrix gives

$$\begin{aligned} \mathbf{P} \nabla \phi(r(\mathbf{x}_k - \mathbf{x})) &= -(\mathbf{P} \cdot \mathbf{x}_k - \mathbf{P} \cdot \mathbf{x}) \frac{1}{r(\mathbf{x}_k - \mathbf{x})} \frac{\partial \phi(r(\mathbf{x}_k - \mathbf{x}))}{\partial r} \\ &= -(\mathbf{P} \cdot \mathbf{x}_k - 0) \frac{1}{r(\mathbf{x}_k - \mathbf{x})} \frac{\partial \phi(r(\mathbf{x}_k - \mathbf{x}))}{\partial r} \\ &= -(I - \mathbf{x} \mathbf{x}^T)(\mathbf{x}_k) \frac{1}{r(\mathbf{x}_k - \mathbf{x})} \frac{\partial \phi(r(\mathbf{x}_k - \mathbf{x}))}{\partial r} \\ &= \begin{pmatrix} x \mathbf{x}^T \mathbf{x}_k - x_k \\ y \mathbf{x}^T \mathbf{x}_k - y_k \\ z \mathbf{x}^T \mathbf{x}_k - z_k \end{pmatrix} \frac{1}{r(\mathbf{x}_k - \mathbf{x})} \frac{\partial \phi(r(\mathbf{x}_k - \mathbf{x}))}{\partial r} \end{aligned}$$

Thus, we directly compute the weights for $P_x \cdot \nabla$ using these three RHS in Equation 3.5:

$$P \frac{\partial}{\partial x_1} = (x_1 \mathbf{x}^T \mathbf{x}_k - x_{1,k}) \frac{1}{r(\mathbf{x}_k - \mathbf{x})} \frac{\partial \phi(r(\mathbf{x}_k - \mathbf{x}))}{\partial r} \Big|_{\mathbf{x}=\mathbf{x}_j} \quad (3.13)$$

$$P \frac{\partial}{\partial x_2} = (x_2 \mathbf{x}^T \mathbf{x}_k - x_{2,k}) \frac{1}{r(\mathbf{x}_k - \mathbf{x})} \frac{\partial \phi(r(\mathbf{x}_k - \mathbf{x}))}{\partial r} \Big|_{\mathbf{x}=\mathbf{x}_j} \quad (3.14)$$

$$P \frac{\partial}{\partial x_3} = (x_3 \mathbf{x}^T \mathbf{x}_k - x_{3,k}) \frac{1}{r(\mathbf{x}_k - \mathbf{x})} \frac{\partial \phi(r(\mathbf{x}_k - \mathbf{x}))}{\partial r} \Big|_{\mathbf{x}=\mathbf{x}_j} \quad (3.15)$$

Alternatively, assuming weights for operators $\nabla = \frac{\partial}{\partial x_1}, \frac{\partial}{\partial x_2}, \frac{\partial}{\partial x_3}$ are already computed, the projected operator could be constructed via weighting the unprojected gradient components. For example:

[Author's Note: Show accuracy of derivative approximation when using projected operator vs linear combinations of dx,dy,dz operators](#)

3.5 Stabilization: Hyperviscosity

For RBF-FD, differentiation matrices encode convective operators of the form

$$D = \alpha \frac{\partial}{\partial \lambda} + \beta \frac{\partial}{\partial \theta} \quad (3.16)$$

where α and β are a function of the fluid velocity. The convective operator, discretized through RBF-FD, has eigenvalues in the right half-plane causing the method to be unstable [25, 18]. Stabilization of the RBF-FD method is achieved through the application of a hyperviscosity filter to Equation (3.16)

[25]. By using Gaussian RBFs, $\phi(r) = e^{-(\epsilon r)^2}$, the hyperviscosity (a high order Laplacian operator) simplifies to

$$\Delta^k \phi(r) = \epsilon^{2k} p_k(r) \phi(r) \quad (3.17)$$

where k is the order of the Laplacian and $p_k(r)$ are multiples of generalized Laguerre polynomials that are generated recursively (see [25]: Section 3.2). We assume a 2D Laplacian operator when working on the surface of the sphere since a local stencil can be viewed as lying on a plane.

In the case of parabolic and hyperbolic PDEs, hyperviscosity is added as a filter to the right hand side of the evaluation. For example, at the continuous level, the equation solved takes the form

$$\frac{\partial u}{\partial t} = -Du + Hu, \quad (3.18)$$

where D is the PDE operator, and H is the hyperviscosity filter operator. Applying hyperviscosity shifts all the eigenvalues of D to the left half of the complex plane. This shift is controlled by k , the order of the Laplacian, and a scaling parameter γ_c , defined by

$$H = \gamma \Delta^k = \gamma_c N^{-k} \Delta^k.$$

Given a choice of ϵ (see Section ??), it was found experimentally that $\gamma = \gamma_c N^{-k}$ provides stability and good accuracy for all values of N considered here. It also ensures that the viscosity vanishes as $N \rightarrow \infty$ [18]. In general, the larger the stencil size, the higher the order of the Laplacian. This is attributed to the fact that, for convective operators, larger stencils treat a wider range of modes accurately. As a result, the hyperviscosity operator should preserve as much of that range as possible. The parameter γ_c must also be chosen with care and its sign depends on k (for k even, γ_c will be negative and for k odd, it will be positive). If γ_c is too large, the eigenvalues move outside the stability domain of our time-stepping scheme and/or eigenvalues corresponding to lower physical modes are not left intact, reducing the accuracy of our approximation. If γ_c is too small, eigenvalues remain in the right half-plane [25, 18].

Chapter 4

TEMP

4.1 Fragments (integrate above)

Stabilization of the RBF-FD method is achieved through the application of a hyperviscosity filter [?]. By assuming the use of Gaussian RBFs, $\phi(r) = e^{-(\epsilon r)^2}$, the hyperviscosity operator simplifies to

$$\Delta^k \phi(r) = \epsilon^{2k} p_k(r) \phi(r). \quad (4.1)$$

The multiples of generalized Laguerre polynomials, $p_k(r)$, are obtained through the following recursive relation:

$$\begin{cases} p_0(r) &= 1, \\ p_1(r) &= 4(\epsilon r)^2 - 2d, \\ p_k(r) &= 4((\epsilon r)^2 - 2(k-1) - \frac{d}{2})p_{k-1}(r) - 8(k-1)(2(k-1) - 2 + d)p_{k-2}(r), \quad k = 2, 3, \dots \end{cases}$$

where d is the dimension of the problem. We assume $d = 2$ below when working on the surface of the sphere.

Many algorithms exist to query the k -nearest neighbors (equivalently all nodes in the minimum/smallest enclosing circle). Some algorithms overlay a grid similar to Locality Sensitive Hashing and query such as... [?].

Conditioning

Conditioning is defined as:

With condition number estimates we can choose a proper support parameter for uniformly distributed node sets.

Alternative algorithms exist for solving for RBF-FD weights when the systems are overly ill-conditioned. Currently, we have an unpublished algorithm ContourSVD available to play with (demonstrate accuracy improvements).

Node Placement – Centroidal Voronoi Tessellation

We make the assumption for now that we use regularly distributed nodes. Centroidal Voronoi tessellations provide reasonably good distributions for solutions. Examples (heat ellipse, ellipsoid, sphere, square cavity).

The motivation behind RBF-FD is generality/functionality in the numerical method. Scattered nodes are supported. Distribution requires proper choice of support, and tight nodes result in increased conditioning

4.2 Approximate Nearest Neighbor (ANN) Query

RBF methods are traditionally described as general and meshless in that they apply to unstructured clouds of points in arbitrary dimensions. However, although the term meshless implies a method capable of operating with no node connectivity, all numerical methods—meshless RBF methods included—connect nodes in the domain. For example, the “meshless” global RBF method connects every node in the domain to all other nodes. Compact support or local RBF methods like RBF-FD limit connections to nodes that lie within a predetermined radius.

The connections between nodes form a directed adjacency graph with edges that dictate the paths along which data/phenomena can travel. For example, a plus shaped stencil of five points with a center node and four neighboring nodes allows values to propagate north, south, east and west; not northeast, southeast, etc.

They are robust and function on scattered point clouds. RBF-FD in particular requires stencils to be generated from n nearest neighbors to a stencil center. The cost of these neighbor queries can vary greatly depending on the choice of algorithm or data-structure used to make the query.

For example, in general brute force is inefficient. The author of [13] queries n nearest neighbors for a compact-support RBF partition of unity example with a k -D tree. In [18, 25] a k -D Tree is leveraged for all neighbor queries for RBF-FD.

In our work in [3] an alternative to k -D tree was leveraged, based loosely on Locality Sensitive Hashing.

4.2.1 k -D Tree

Most of the RBF community leverages the k -D tree, due to its low computational complexity for querying neighbors and its wide availability as standalone software in the public domain (e.g., matlab central has a few implementations for download, and the MATLAB Statistics Toolbox includes an efficient k -D Tree).

The complexity of assembling the tree is

The Matlab central k -D Tree is MEX compiled and efficient. We integrated the standalone C++ code into our library.

While the k -D Tree functions well for queries, its downfall is a large cost in preprocessing to build the tree. For moving nodes, such as in Lagrangian schemes, this cost is prohibitively high. In an attempt to reduce the cost, lagrangian schemes introduced approximate nearest neighbor queries based on

Approximate nearest neighbors will be nearly balanced. We observe that RBF-FD functions as well on stencils of true nearest neighbors as it does on approximate nearest neighbors.

Chapter 5

Distributed/Parallel RBF Methods

RBFs on GPU work: [\[44, 45\]](#) (global), [\[62\]](#) (compact)

Part III

Appendices

The following appendices are included to illuminate subtleties of the RBF-FD method. The first discusses the method's ability to avoid pole singularities when applied to solid body transport on the sphere. The second considers the difference between directly computing weights for differentiation operators versus leveraging linear combinations of weights to indirectly construct the same operators.

Appendix A

Avoiding Pole Singularities with RBF-FD

This content follows [19, 20].

Within the test cases of this dissertation, we solve convective PDEs on the unit sphere with the form:

$$\frac{\partial h}{\partial t} = \mathbf{u} \cdot \nabla h$$

where \mathbf{u} is velocity. For example, the cosine bell advection has this particular form:

$$\frac{\partial h}{\partial t} = \frac{u}{\cos \theta} \frac{\partial h}{\partial \lambda} + v \frac{\partial h}{\partial \theta} \quad (\text{A.1})$$

in the spherical coordinate system defined by

$$\begin{aligned} x &= \cos \theta \cos \lambda \\ y &= \cos \theta \sin \lambda \\ z &= \sin \theta \end{aligned}$$

where $\theta \in (-\frac{\pi}{2}, \frac{\pi}{2})$ is the elevation angle and $\lambda \in (-\pi, \pi)$ is the azimuthal angle. Observe that as $\theta \rightarrow \pm \frac{\pi}{2}$, the $\frac{1}{\cos \theta}$ term goes to infinity as a discontinuity.

One of the many selling points for RBF-FD and other RBF methods is their ability analytically avoid pole singularities, which arise from the choice of coordinate system and not from the methods themselves. Since RBFs are inherently based on Euclidean distance between nodes, and not geodesic distance, it is said that they do not “feel” the effects of the geometry or recognize singularities naturally inherent in the coordinate system [19]. Here we demonstrate how pole singularities are analytically avoided with RBF-FD for cosine bell advection.

Let $r = \|\mathbf{x} - \mathbf{x}_j\|$ be the Euclidean distance which is invariant of the coordinate system. In Cartesian coordinates, we have

$$r = \sqrt{(x - x_j)^2 + (y - y_j)^2 + (z - z_j)^2}.$$

In spherical coordinates we have:

$$r = \sqrt{2(1 - \cos \theta \cos \theta_j \cos(\lambda - \lambda_j) - \sin \theta \sin \theta_j)}.$$

The RBF-FD operators for $\frac{d}{d\lambda}$, $\frac{d}{d\theta}$ are discretized with the chain rule:

$$\frac{d\phi_j(r)}{d\lambda} = \frac{dr}{d\lambda} \frac{d\phi_j(r)}{dr} = \frac{\cos \theta \cos \theta_j \sin(\lambda - \lambda_j)}{r} \frac{d\phi_j(r)}{dr}, \quad (\text{A.2})$$

$$\frac{d\phi_j(r)}{d\theta} = \frac{dr}{d\theta} \frac{d\phi_j(r)}{dr} = \frac{\sin \theta \cos \theta_j \cos(\lambda - \lambda_j) - \cos \theta \sin \theta_j}{r} \frac{d\phi_j(r)}{dr}, \quad (\text{A.3})$$

where $\phi_j(r)$ is the RBF centered at \mathbf{x}_j .

Plugging [A.2](#) and [A.3](#) into [A.1](#), produces the following explicit form:

$$\frac{dh}{dt} = u(\cos \theta_j \sin(\lambda - \lambda_j) \frac{1}{r} \frac{d\phi_j}{dr}) + v(\sin \theta \cos \theta_j \cos(\lambda - \lambda_j) - \cos \theta \sin \theta_j \frac{1}{r} \frac{d\phi_j}{dr})$$

where $\cos \theta$ from [A.2](#) analytically cancels with the $\frac{1}{\cos \theta}$ in [A.1](#).

Then, formally, one would assemble differentiation matrices containing weights for the following operators:

$$\mathbf{D}_\lambda = \cos \theta_j \sin(\lambda - \lambda_j) \frac{1}{r} \frac{d\phi_j}{dr}, \quad (\text{A.4})$$

$$\mathbf{D}_\theta = \sin \theta \cos \theta_j \cos(\lambda - \lambda_j) - \cos \theta \sin \theta_j \frac{1}{r} \frac{d\phi_j}{dr}, \quad (\text{A.5})$$

and solve the explicit method of lines problem:

$$\frac{dh}{dt} = u\mathbf{D}_\lambda h + v\mathbf{D}_\theta h$$

where now the system is completely free of singularities at the poles [\[20\]](#).

We note that the expression $\cos(\frac{\pi}{2})$ evaluates on some systems to a very small number rather than zero (e.g., $6.1(10^{-17})$ on the Keeneland system with the GNU gcc compiler). The small value in turn allows $\frac{1}{\cos \theta}$ to evaluate to a large value (e.g., $1.6(10^{16})$) rather than “inf” or “NaN”. A large value allows the cosine terms to cancel in double precision, whereas an “inf” or “NaN” would corrupt the numerics. Rather than avoid placing nodes at the poles, or assuming the machine will numerically cancel the singularities, it is preferred to use operators [A.4](#), [A.5](#) on the RHS of Equation [3.5](#) to compute RBF-FD weights.

Appendix B

Projected Weights on the Sphere

It is shown in [20, 18] that a projection operator

$$\mathbf{P} = \mathbf{I} - \mathbf{x}\mathbf{x}^T = \begin{bmatrix} (1-x^2) & -xy & -xz \\ -xy & (1-y^2) & -yz \\ -xz & -yz & (1-z^2) \end{bmatrix} = \begin{bmatrix} \mathbf{p}_x^T \\ \mathbf{p}_y^T \\ \mathbf{p}_z^T \end{bmatrix}$$

where \mathbf{p}_x^T represents the projection operator in the x direction.

From [20], the projected RBF gradient operator is:

$$\begin{aligned} \mathbf{P} \cdot \nabla \phi_k(r(\mathbf{x})) &= \mathbf{P} \cdot \frac{(\mathbf{x} - \mathbf{x}_k)}{r(\mathbf{x})} \frac{d\phi_k(r(\mathbf{x}))}{dr(\mathbf{x})} \\ &= -\mathbf{P} \cdot \mathbf{x}_k \frac{1}{r(\mathbf{x})} \frac{d\phi_k(r(\mathbf{x}))}{dr(\mathbf{x})} \\ &= \begin{bmatrix} x\mathbf{x}^T \mathbf{x}_k - x_k \\ y\mathbf{x}^T \mathbf{x}_k - y_k \\ z\mathbf{x}^T \mathbf{x}_k - z_k \end{bmatrix} \frac{1}{r(\mathbf{x})} \frac{d\phi(r(\mathbf{x}))}{dr}. \end{aligned} \quad (\text{B.1})$$

The operator $\mathbf{I} - \mathbf{x}\mathbf{x}^T$ for $\mathbf{x} = (x, y, z)$ projects a vector onto the plane tangent to the unit sphere at (x, y, z) . Therefore, Equation B.1 gives the projection of the gradient operator at \mathbf{x}_k onto the plane tangent to \mathbf{x} .

B.1 Direct Weights

Following [18], B.1 takes on the following when adapted to RBF-FD:

$$[\mathbf{p}_x \cdot \nabla f(\mathbf{x})]|_{\mathbf{x}=\mathbf{x}_c} = \sum_{k=1}^n c_k \underbrace{[x_c \mathbf{x}_c^T \mathbf{x}_k - x_k]}_{B_{c,k}^{\mathbf{p}_x}} \frac{1}{r} \frac{d\phi(r(x_c))}{dr}. \quad (\text{B.2})$$

and so forth for the $\mathbf{p}_y \cdot \nabla, \mathbf{p}_z \cdot \nabla$ operators, where \mathbf{x}_c is the stencil center and \mathbf{x}_k are stencil nodes. To compute RBF-FD weights for the $\mathbf{p}_x \cdot \nabla$ operator, the RHS of Equation 3.5 is filled with elements $B_{c,k}^{\mathbf{p}_x}$. We will refer to this method of obtaining the weights as the *direct* method due to the ability to directly compute RBF-FD weights for the operators $\mathbf{P} \cdot \nabla$, and assemble the differentiation matrices $\mathbf{D}_{\mathbf{p}_x \cdot \nabla}, \mathbf{D}_{\mathbf{p}_y \cdot \nabla}, \mathbf{D}_{\mathbf{p}_z \cdot \nabla}$ without the need to compute and/or store other weights.

B.2 Indirect Weights

Alternatively, one is able to compute weights *indirectly* as a weighted combination of existing RBF-FD weights for the unprojected ∇ operator. Here we assume that differentiation matrices to compute the components of ∇ are readily available in memory:

$$\mathbf{D}_{\nabla} = \begin{bmatrix} \mathbf{D}_{\frac{d}{dx}} \\ \mathbf{D}_{\frac{d}{dy}} \\ \mathbf{D}_{\frac{d}{dz}} \end{bmatrix},$$

where each matrix contains weights computed with the operators of Equation ?? applied to the RHS of Equation 3.5.

The differentiation matrices for $\mathbf{P} \cdot \nabla$ can then be assembled as a weighted combination of the differentiation matrices for the unprojected operator:

$$\mathbf{D}_{\mathbf{P} \cdot \nabla} = \begin{bmatrix} \mathbf{D}_{\mathbf{P}_x \cdot \nabla} \\ \mathbf{D}_{\mathbf{P}_y \cdot \nabla} \\ \mathbf{D}_{\mathbf{P}_z \cdot \nabla} \end{bmatrix} = \begin{bmatrix} \text{diag}(1 - X^2) \mathbf{D}_{\frac{\partial x}{\partial x}} - \text{diag}(XY) \mathbf{D}_{\frac{d}{dy}} - \text{diag}(XZ) \mathbf{D}_{\frac{d}{dz}} \\ -\text{diag}(XY) \mathbf{D}_{\frac{d}{dx}} + \text{diag}(1 - Y^2) \mathbf{D}_{\frac{d}{dy}} - \text{diag}(YZ) \mathbf{D}_{\frac{d}{dz}} \\ -\text{diag}(XZ) \mathbf{D}_{\frac{d}{dx}} - \text{diag}(YZ) \mathbf{D}_{\frac{d}{dy}} + \text{diag}(1 - Y^2) \mathbf{D}_{\frac{d}{dz}} \end{bmatrix} \quad (\text{B.3})$$

Author's Note: make it "partial x" instead of d/dx where $X = \{x_{c,i}\}_{i=1}^N$, $Y = \{y_{c,i}\}_{i=1}^N$, $Z = \{z_{c,i}\}_{i=1}^N$ are all x-components, y-components and z-components of the stencil centers $\{\mathbf{x}_{c,i}\}_{i=1}^N$ respectively. Author's Note: Gordon discussion: BF: explain why we use this manufactured solution, what was it designed to check. Author's Note: Cleanup: This concept equates to classical Finite Differences where for example, the standard 5-point finite difference formula for approximating the Laplacian can be expressed a weighted combination of differences for

Author's Note: Have not found in literature any mention of the fact that RBF-FD weights can be used to compose operators like this. Generally, its easier to directly compute weights and assumed to be more accurate. But how much more accurate?

One benefit of indirect weights is conservation of memory. For example, for complex operators, a single DM on $N = 1\text{million}$ nodes and $n = 101$ requires roughly 1.6 GB of memory. If the PDE is coupled and requires

This also allows us to compose complex operators with weights loaded from disk

$O(N*n)$ cost to assemble the indirect operators after $O(N*n^3)$ cost of assembling direct operators means this approach has potential to save FLOPs in the long run

But the question is, how accurate is it? In situations where memory is critical and these FLOPs need to be saved (i.e., large N and complicated equations), would it be useful?

Author's Note: Q: how do direct vs indirect weights compare? Is the lsf different sparsity with same approximation potentials? Author's Note: end

B.2.1 Comparison of Direct and Indirect Weights

We computed direct and indirect approaches for the MD-node sets with size $N = \{121, 256, 400, 841, 1024, 2500, 4096, 6400\}$.

We check the relative error of the approximation:

$$\text{relative } \ell_2 \text{ error} = \frac{\|f_{\text{approx}} - f_{\text{exact}}\|_2}{\|f_{\text{exact}}\|_2}$$

We also look at the difference of relative errors and its absolute value:

$$(\text{relative } \ell_2 \text{ error})_{\text{direct}} - (\text{relative } \ell_2 \text{ error})_{\text{indirect}}$$

We find that our indirect approach functions well compared to the direct method. For small node sizes ($N < 2500$ nodes) we see that the direct method has the advantage with

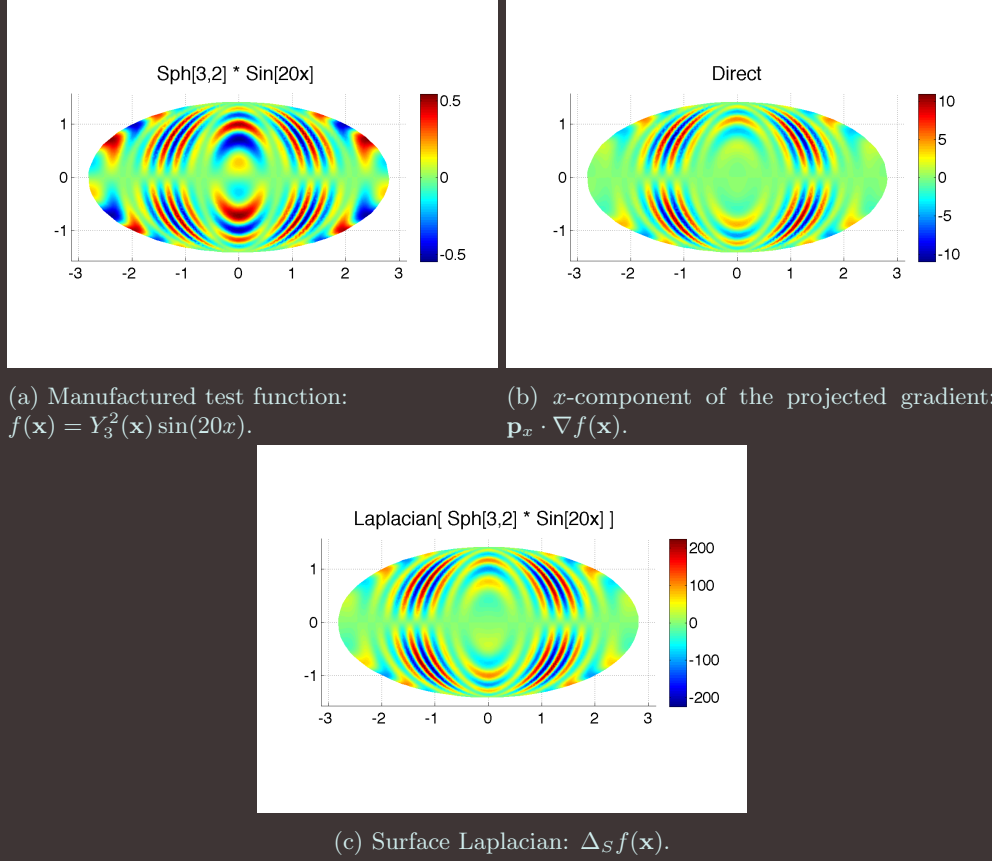
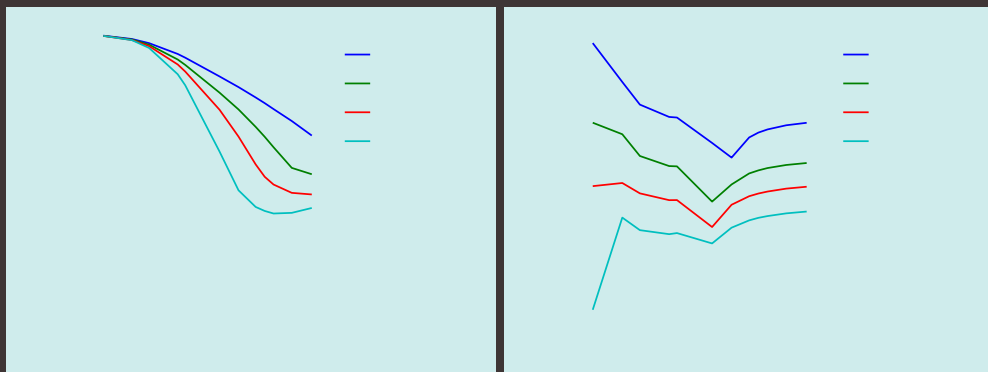


Figure B.1: Test function and its projected derivatives on the surface of the unit sphere.

B.3 Conclusions

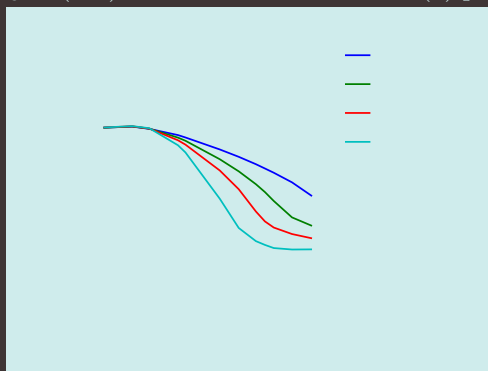
Although it is clear the indirect method functions well compared to the direct method, we must consider its usefulness. Typically, weights are computed only as necessary for the PDE. If the PDE is on the sphere, then directly computing the $\mathbf{P} \cdot \nabla$ operator would be most efficient for both memory and computation. However, one could imagine a scenario such as a 3-D spherical shell domain with physics on the boundaries that must be constrained to the surface, while the interior requires only an unprojected ∇ operator. In such cases, by simply computing for the ∇ operator, we assemble all necessary operators with minimal loss of accuracy and significant savings ($3Nn$ doubles) in storage.

With $N = 1e6$ nodes and stencil size $n = 101$, the matrix market file for weights is approximately 1.6 GB on disk. For a GPU with only 6 GB of global memory space available, it is worthwhile to consider possibilities for memory conservation.



(a) Δ_S of $Y_3^2 \sin(20x)$

(b) $\mathbf{p}_x \cdot \nabla(Y_3^2)$



(c) $\mathbf{p}_x \cdot \nabla(Y_3^2 \sin(20x))$ Author's Note: [rescale 1e0 down to 1e-8](#)

Figure B.2: Relative ℓ_2 error in differentiation.

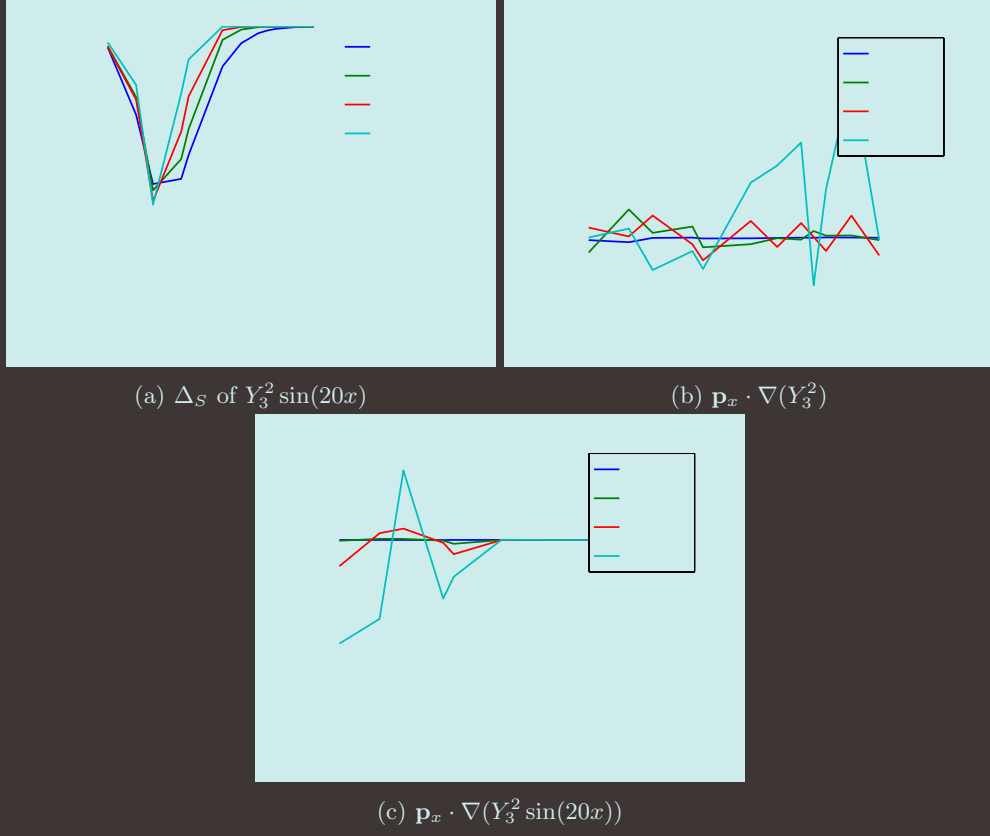


Figure B.3: Signed differences of relative ℓ_2 errors in differentiation between Direct and Indirect weights.

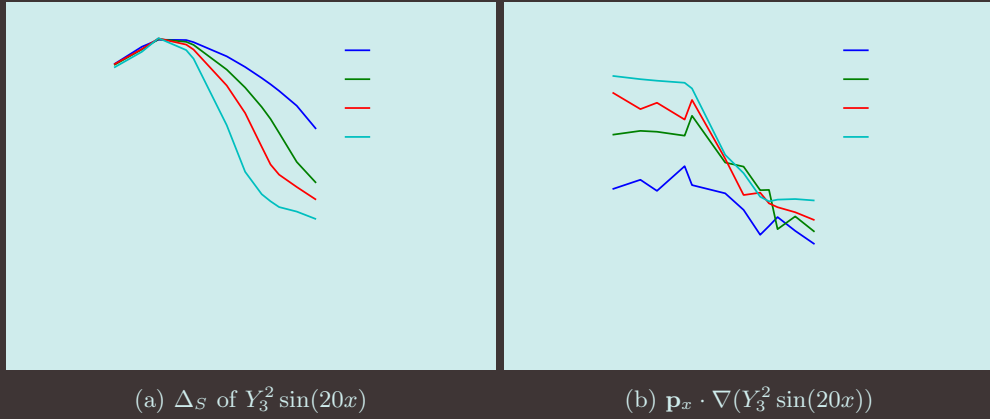


Figure B.4: Absolute differences of relative ℓ_2 errors in differentiation between Direct and Indirect weights.

Bibliography

- [1] Sylvie Barak. Gpu technology key to exascale says nvidia. <http://www.eetimes.com/electronics-news/4230659/GPU-technology-key-to-exascale-says-Nvidia>, November 2011. 18
- [2] R. K. Beatson, W. A. Light, and S. Billings. Fast Solution of the Radial Basis Function Interpolation Equations: Domain Decomposition Methods. *SIAM J. Sci. Comput.*, 22(5):1717–1740, 2000. 17
- [3] Evan F. Bollig, Natasha Flyer, and Gordon Erlebacher. Solution to pdes using radial basis function finite-differences (rbf-fd) on multiple gpus. *Journal of Computational Physics*, (0):–, 2012. 26
- [4] J. C. Carr, R. K. Beatson, J. B. Cherrie, T. J. Mitchell, W. R. Fright, B. C. McCallum, and T. R. Evans. Reconstruction and Representation of 3D Objects with Radial Basis Functions. In *SIGGRAPH '01: Proceedings of the 28th annual conference on Computer graphics and interactive techniques*, pages 67–76, New York, NY, USA, 2001. ACM. 10
- [5] J. C. Carr, R. K. Beatson, B. C. McCallum, W. R. Fright, T. J. McLennan, and T. J. Mitchell. Smooth Surface Reconstruction from Noisy Range Data. In *GRAPHITE '03: Proceedings of the 1st international conference on Computer graphics and interactive techniques in Australasia and South East Asia*, pages 119–ff, New York, NY, USA, 2003. ACM. 10
- [6] Tom Cecil, Jianliang Qian, and Stanley Osher. Numerical Methods for High Dimensional Hamilton-Jacobi Equations Using Radial Basis Functions. *JOURNAL OF COMPUTATIONAL PHYSICS*, 196:327–347, 2004. 7, 8
- [7] G Chandhini and Y Sanyasiraju. Local RBF-FD Solutions for Steady Convection-Diffusion Problems. *International Journal for Numerical Methods in Engineering*, 72(3), 2007. 7, 8
- [8] P P Chinchapatnam, K Djidjeli, P B Nair, and M Tan. A compact RBF-FD based meshless method for the incompressible Navier–Stokes equations. *Proceedings of the Institution of Mechanical Engineers, Part M: Journal of Engineering for the Maritime Environment*, 223(3):275–290, March 2009. 8
- [9] CD Correa, D Silver, and M Chen. Volume Deformation via Scattered Data Interpolation. *Proceedings of Eurographics/IEEE VGTC Workshop on Volume Graphics*, pages 91–98, 2007. 7, 14
- [10] E Divo and AJ Kassab. An Efficient Localized Radial Basis Function Meshless Method for Fluid Flow and Conjugate Heat Transfer. *Journal of Heat Transfer*, 129:124, 2007. 7, 14, 17
- [11] G. E. Fasshauer. RBF Collocation Methods and Pseudospectral Methods. Technical report, 2006. 3, 6, 7, 13

- [12] Gregory E. Fasshauer. Solving Partial Differential Equations by Collocation with Radial Basis Functions. In *In: Surface Fitting and Multiresolution Methods A. Le M'ehaut'e, C. Rabut and L.L. Schumaker (eds.), Vanderbilt*, pages 131–138. University Press, 1997. 5, 7, 11, 12
- [13] Gregory E. Fasshauer. *Meshfree Approximation Methods with MATLAB*, volume 6 of *Interdisciplinary Mathematical Sciences*. World Scientific Publishing Co. Pte. Ltd., 5 Toh Tuck Link, Singapore 596224, 2007. 3, 6, 7, 9, 11, 13, 26
- [14] Gregory E. Fasshauer and Jack G. Zhang. On choosing “optimal” shape parameters for rbf approximation. *Numerical Algorithms*, 45(1-4):345–368, 2007. 6
- [15] A. I. Fedoseyev, M. J. Friedman, and E. J. Kansa. Improved Multiquadric Method for Elliptic Partial Differential Equations via PDE Collocation on the Boundary. *Computers & Mathematics with Applications*, 43(3-5):439 – 455, 2002. 5, 6, 7, 12
- [16] Natasha Flyer and Bengt Fornberg. Radial basis functions: Developments and applications to planetary scale flows. *Computers & Fluids*, 46(1):23–32, July 2011. 2, 6, 7
- [17] Natasha Flyer and Erik Lehto. Rotational transport on a sphere: Local node refinement with radial basis functions. *Journal of Computational Physics*, 229(6):1954–1969, March 2010. 2
- [18] Natasha Flyer, Erik Lehto, Sebastien Blaise, Grady B. Wright, and Amik St-Cyr. Rbf-generated finite differences for nonlinear transport on a sphere: shallow water simulations. *Submitted to Elsevier*, pages 1–29, 2011. 8, 21, 22, 23, 24, 26, 32
- [19] Natasha Flyer and Grady B. Wright. Transport schemes on a sphere using radial basis functions. *Journal of Computational Physics*, 226(1):1059 – 1084, 2007. 2, 6, 7, 30
- [20] Natasha Flyer and Grady B. Wright. A Radial Basis Function Method for the Shallow Water Equations on a Sphere. In *Proc. R. Soc. A*, volume 465, pages 1949–1976, December 2009. 2, 6, 7, 22, 23, 30, 31, 32
- [21] B Fornberg, T Driscoll, G Wright, and R Charles. Observations on the behavior of radial basis function approximations near boundaries. *Computers & Mathematics with Applications*, 43(3-5):473–490, February 2002. 21
- [22] B. Fornberg and G. Wright. Stable computation of multiquadric interpolants for all values of the shape parameter. *Computers & Mathematics with Applications*, 48(5-6):853 – 867, 2004. 3, 7, 17
- [23] Bengt Fornberg, Elisabeth Larsson, and Natasha Flyer. Stable Computations with Gaussian Radial Basis Functions in 2-D. Technical Report 2009-020, Uppsala University, August 2009. 17
- [24] Bengt Fornberg, Elisabeth Larsson, and Natasha Flyer. Stable Computations with Gaussian Radial Basis Functions. *SIAM J. on Scientific Computing*, 33(2):869—892, 2011. 3, 17
- [25] Bengt Fornberg and Erik Lehto. Stabilization of RBF-generated finite difference methods for convective PDEs. *Journal of Computational Physics*, 230(6):2270–2285, March 2011. 8, 21, 23, 24, 26
- [26] Bengt Fornberg and Cécile Piret. A Stable Algorithm for Flat Radial Basis Functions on a Sphere. *SIAM Journal on Scientific Computing*, 30(1):60–80, 2007. 3, 17
- [27] Bengt Fornberg and Cécile Piret. On Choosing a Radial Basis Function and a Shape Parameter when Solving a Convective PDE on a Sphere. *Journal of Computational Physics*, 227(5):2758 – 2780, 2008. 3, 7

- [28] Richard Franke. Scattered Data Interpolation: Tests of Some Method. *Mathematics of Computation*, 38(157):181–200, 1982. [3](#), [7](#)
- [29] Prashant Goswami, Philipp Schlegel, Barbara Solenthaler, and Renato Pajarola. Interactive sph simulation and rendering on the gpu. In *Proceedings of the 2010 ACM SIGGRAPH/Eurographics Symposium on Computer Animation*, SCA '10, pages 55–64, Aire-la-Ville, Switzerland, Switzerland, 2010. Eurographics Association. [21](#)
- [30] R Hardy. Multiquadratic Equations of Topography and Other Irregular Surfaces. *J. Geophysical Research*, (76):1–905, 1971. [2](#), [3](#)
- [31] Y. C. Hon and R. Schaback. On unsymmetric collocation by radial basis functions. *Appl. Math. Comput.*, 119(2-3):177–186, 2001. [5](#), [6](#), [7](#), [9](#)
- [32] Yiu-Chung Hon, Kwok Fai Cheung, Xian-Zhong Mao, and Edward J. Kansa. A Multiquadric Solution for the Shallow Water Equations. *ASCE J. Hydraulic Engineering*, 125:524–533, 1999. [6](#), [7](#)
- [33] A. Iske. *Multiresolution Methods in Scattered Data Modeling*. Springer, 2004. [3](#), [7](#), [9](#)
- [34] E J Kansa. Multiquadrics—A scattered data approximation scheme with applications to computational fluid-dynamics. I. Surface approximations and partial derivative estimates. *Computers Math. Applic*, (19):127–145, 1990. [2](#), [3](#), [5](#), [7](#), [11](#)
- [35] E J Kansa. Multiquadrics—A scattered data approximation scheme with applications to computational fluid-dynamics. II. Solutions to parabolic, hyperbolic and elliptic partial differential equations. *Computers Math. Applic*, (19):147–161, 1990. [2](#), [3](#), [5](#), [7](#), [11](#)
- [36] G Kosec and B Šarler. Solution of thermo-fluid problems by collocation with local pressure correction. *International Journal of Numerical Methods for Heat & Fluid Flow*, 18, 2008. [7](#), [17](#)
- [37] Elisabeth Larsson and Bengt Fornberg. A Numerical Study of some Radial Basis Function based Solution Methods for Elliptic PDEs. *Comput. Math. Appl*, 46:891–902, 2003. [3](#), [5](#), [6](#), [7](#), [11](#), [12](#), [17](#)
- [38] Yuxu Lin, Chun Chen, Mingli Song, and Zicheng Liu. Dual-RBF based surface reconstruction. *Vis Comput*, 25(5-7):599–607, May 2009. [7](#), [14](#)
- [39] X. Liu, G.R. Liu, K. Tai, and K.Y. Lam. Radial point interpolation collocation method (RPICM) for partial differential equations. *Computers & Mathematics with Applications*, 50(8-9):1425 – 1442, 2005. [7](#), [14](#)
- [40] Bryan S. Morse, Terry S. Yoo, Penny Rheingans, David T. Chen, and K. R. Subramanian. Interpolating implicit surfaces from scattered surface data using compactly supported radial basis functions. In *ACM SIGGRAPH 2005 Courses*, SIGGRAPH '05, New York, NY, USA, 2005. ACM. [6](#), [7](#)
- [41] C.T. Mouat and R.K. Beatson. RBF Collocation. Technical Report UCDMS2002/3, Department of Mathematics & Statistics, University of Canterbury, New Zealand, February 2002. [7](#), [8](#), [11](#)
- [42] Jia Pan and Dinesh Manocha. Fast GPU-based Locality Sensitive Hashing for K-Nearest Neighbor Computation. *Proceedings of the 19th ACM SIGSPATIAL GIS '11*, 2011. [21](#)
- [43] Robert Schaback. Multivariate Interpolation and Approximation by Translates of a Basis Function. In C.K. Chui and L.L. Schumaker, editors, *Approximation Theory VIII—Vol. 1: Approximation and Interpolation*, pages 491–514. World Scientific Publishing Co., Inc, 1995. [3](#), [8](#)

- [44] J. Schmidt, C. Piret, B.J. Kadlec, D.A. Yuen, E. Sevre, N. Zhang, and Y. Liu. Simulating Tsunami Shallow-Water Equations with Graphics Accelerated Hardware (GPU) and Radial Basis Functions (RBF). In *South China Sea Tsunami Workshop*, 2008. 27
- [45] J. Schmidt, C. Piret, N. Zhang, B.J. Kadlec, D.A. Yuen, Y. Liu, G.B. Wright, and E. Sevre. Modeling of Tsunami Waves and Atmospheric Swirling Flows with Graphics Processing Unit (GPU) and Radial Basis Functions (RBF). *Concurrency and Computat.: Pract. Exper.*, 2009. 7, 27
- [46] C. Shu, H. Ding, and K. S. Yeo. Local radial basis function-based differential quadrature method and its application to solve two-dimensional incompressible Navier-Stokes equations. *Computer Methods in Applied Mechanics and Engineering*, 192(7-8):941 – 954, 2003. 7, 8
- [47] C Shu, H Ding, and N Zhao. Numerical Comparison of Least Square-Based Finite-Difference (LSFD) and Radial Basis Function-Based Finite-Difference (RBF-FD) Methods. *Computers and Mathematics with Applications*, 51(8):1297–1310, 2006. 7, 8, 17
- [48] D Stevens, H Power, M Lees, and H Morvan. The use of PDE centres in the local RBF Hermitian method for 3D convective-diffusion problems. *Journal of Computational Physics*, 2009. 5, 7, 8, 12, 14
- [49] David Stevens, Henry Power, Michael Lees, and Herve Morvan. A Meshless Solution Technique for the Solution of 3D Unsaturated Zone Problems, Based on Local Hermitian Interpolation with Radial Basis Functions. *Transp Porous Med*, 79(2):149–169, Sep 2008. 7, 14
- [50] David Stevens, Henry Power, and Herve Morvan. An order-N complexity meshless algorithm for transport-type PDEs, based on local Hermitian interpolation. *Engineering Analysis with Boundary Elements*, 33(4):425 – 441, 2008. 7, 14, 17
- [51] A. I. Tolstykh and D. A. Shirobokov. On using radial basis functions in a “finite difference mode” with applications to elasticity problems. In *Computational Mechanics*, volume 33, pages 68 – 79. Springer, December 2003. 7
- [52] A.I. Tolstykh. On using RBF-based differencing formulas for unstructured and mixed structured-unstructured grid calculations. In *Proceedings of the 16 IMACS World Congress, Lausanne*, pages 1–6, 2000. 7
- [53] Robert Vertnik and Božidar Šarler. Meshless local radial basis function collocation method for convective-diffusive solid-liquid phase change problems. *International Journal of Numerical Methods for Heat & Fluid Flow*, 16(5):617–640, 2006. 7, 14
- [54] B. Šarler and R. Vertnik. Meshfree Explicit Local Radial Basis Function Collocation Method for Diffusion Problems. *Computers and Mathematics with Applications*, 51(8):1269–1282, 2006. 7, 14
- [55] J. G. Wang and G. R. Liu. A point interpolation meshless method based on radial basis functions. *Int. J. Numer. Methods Eng.*, 54, 2002. 7, 14
- [56] Grady Wright and Bengt Fornberg. Scattered node mehrstellenverfahren-type formulas generated from radial basis functions. In *The International Conference on Computational Methods*, December 15-17 2004. 7, 8
- [57] Grady B. Wright. *Radial Basis Function Interpolation: Numerical and Analytical Developments*. PhD thesis, University of Colorado, 2003. 7, 8, 14

- [58] Grady B. Wright, Natasha Flyer, and David A. Yuen. A hybrid radial basis function–pseudospectral method for thermal convection in a 3-d spherical shell. *Geochem. Geophys. Geosyst.*, 11(Q07003):18 pp., 2010. [2](#), [6](#), [7](#), [13](#), [22](#)
- [59] Grady B. Wright and Bengt Fornberg. Scattered node compact finite difference-type formulas generated from radial basis functions. *J. Comput. Phys.*, 212(1):99–123, 2006. [7](#), [8](#), [21](#)
- [60] Z M Wu. Hermite-Birkhoff interpolation of scattered data by radial basis functions. *Approx. Theory Appl*, (8):1–10, 1992. [5](#)
- [61] Xuan Yang, Zhixiong Zhang, and Ping Zhou. Local Elastic Registration of Multimodal Medical Image Using Robust Point Matching and Compact Support RBF. In *BMEI '08: Proceedings of the 2008 International Conference on BioMedical Engineering and Informatics*, pages 113–117, Washington, DC, USA, 2008. IEEE Computer Society. [7](#), [14](#)
- [62] Rio Yokota, L.A. Barba, and Matthew G. Knepley. PetRBF — A parallel O(N) algorithm for radial basis function interpolation with Gaussians. *Computer Methods in Applied Mechanics and Engineering*, 199(25-28):1793–1804, May 2010. [27](#)
- [63] Hao Zhang and Marc G. Genton. Compactly supported radial basis function kernels, 2004. [7](#)